



HAL
open science

Effect of climate on asphalt pavement performance using two mechanistic-empirical methods

Rahma Ktari, Denis Saint-Laurent, Pierre Hornych, Ferhat Hammoum, Paul Marsac, Mai Lan Nguyen

► To cite this version:

Rahma Ktari, Denis Saint-Laurent, Pierre Hornych, Ferhat Hammoum, Paul Marsac, et al.. Effect of climate on asphalt pavement performance using two mechanistic-empirical methods. International Journal of Pavement Engineering, 2020, 27 p. 10.1080/10298436.2020.1806276 . hal-02942289

HAL Id: hal-02942289

<https://hal.science/hal-02942289>

Submitted on 8 Jun 2021

HAL is a multi-disciplinary open access archive for the deposit and dissemination of scientific research documents, whether they are published or not. The documents may come from teaching and research institutions in France or abroad, or from public or private research centers.

L'archive ouverte pluridisciplinaire **HAL**, est destinée au dépôt et à la diffusion de documents scientifiques de niveau recherche, publiés ou non, émanant des établissements d'enseignement et de recherche français ou étrangers, des laboratoires publics ou privés.

Effect of climate on asphalt pavement performance using two mechanistic-empirical methods

Rahma KTARI¹, Denis SAINT-LAURENT², Pierre HORNYCH^{1*}, Ferhat HAMMOUM¹, Paul MARSAC¹, Mai Lan NGUYEN¹

¹IFSTTAR, MAST, F-44344 Bouguenais, France, * pierre.hornych@ifsttar.fr

²Ministère des Transports Québec (MTQ), Direction des chaussées, 800, place D'Youville, 14^e étage, Québec (Québec) G1R 3P4, denis.st-laurent@transport.gouv.qc.ca

Highlights

- Presentation of two mechanistic-empirical (ME) methods for pavement design
- Description of the fatigue equations governing asphalt mixes for design purposes
- Identification of the parameters used in the design of pavement structures
- Study of the influence of the climate in France and Québec on pavement performance
- Comparison of the French and US methods for pavement design and correspondence between them

Abbreviations

- AASHTO: American Association of State Highway and Transportation Officials
- AC: Asphalt Concrete
- EICM: Enhanced Integrated Climatic Model
- EME: "enrobé à module élevé" or high modulus asphalt
- ESG: "enrobé semi-grenu", or medium-coarse asphalt
- FHWA: Federal Highway Administration
- GB: "grave-bitume", or gravel/bitumen mix
- IFSTTAR: Institut français des sciences et technologies des transports, de l'aménagement et des réseaux
- IRI: International Roughness Index
- LTPP: Long-Term Pavement Performance
- MAAT: Mean annual air temperature

- MAST: Département Matériaux et Structures
- MEPDG: Mechanistic-Empirical Pavement Design Guide
- MIT: Matériaux pour Infrastructures de Transports
- MOP: Manual of Practice
- MTQ: Ministère des Transports du Québec
- NCHRP: National Cooperative Highway Research Program
- PF: "plateforme", or working platform
- PMED: Pavement Mechanistic-Empirical (ME) Design

Abstract

The objective of this study is to assess the impact of climate on the performance of bituminous pavements with two different methods, and then to examine their impact on actual design scenarios. Three climate cases were selected for the comparisons involving the effect of temperature: one in France (Bordeaux) and two in the United States (Seattle and Phoenix). The case of an experimental site in Québec was also used for comparisons concerning consideration for seasonal variations in ground bearing capacity. The analyses used two mechanistic-empirical approaches: the French method (NF P98-086 standard, LCPC-SETRA 1994 handbook, and the Alizé-LCPC software package) and the US method (NCHRP 2004 guide, AASHTO 2015 manual of practice, and the AASHTOWare Pavement ME Design software package). The results of the study highlight the importance, for design purposes, of the empirical fatigue equations as a function of temperature. For the site studied in France, the design results in terms of AC base layer thicknesses indicate that both methods show a similar trend with an increase in temperature. For the site in Québec, which is submitted to severe freeze/thaw cycles, the results show that taking temperature and moisture into account for unbound materials leads to a prediction of more severe permanent deformation.

Keywords

Mechanistic-empirical pavement design, asphalt concrete, performance, fatigue, temperature, climate.

1. Introduction

Bituminous pavement design is one of the key elements in the lifecycle of road infrastructures, and has economic, technical, societal and environmental implications. The main climate parameters that may influence road stability are temperature and water or precipitation. The use of climate data makes it possible to predict the behaviour of asphalt mixes in response to temperature and to anticipate the moisture contents and stiffness variations of underlying unbound materials. Temperature is an important factor that must be taken into account when designing a pavement structure. In warm periods, high temperatures soften asphalt mixes. For soils and untreated granular materials, the focus shifts to the variations in moisture and ice contents caused by water or precipitation, and freeze/thaw cycles in northern climates.

The identification of the climate-related mechanisms driving pavement degradation are an important research topic that can help optimize investment in the construction, maintenance and repair of the road network. Some countries, including Canada, face significant seasonal temperature variations, from $-30\text{ }^{\circ}\text{C}$ in winter to $+30\text{ }^{\circ}\text{C}$ in summer. These variations, combined with heavy traffic, lead to permanent deformation, structural fatigue cracking and thermal cracking.

This study is part of a project funded by the Pays de Loire region in France, entitled "Réseau International RI-ADAPTCLIM". Its goal is to assess risks and improve the climate adaptation of infrastructures and civil engineering works. The first objective of this study is to assess the impact of climate on the performance and design of two existing bituminous pavement sections, one in France and one in Canada. More specifically, the study focuses on the effects of temperature and moisture on the performance and design of bituminous pavements. The second objective is to study these issues with the French and the US mechanistic-empirical pavement design methods, and to explore possible ways to connect them. The study is divided into seven sections.

This introduction is followed by the second section, which reviews recent studies looking at the effect of the climate on pavement design.

The third section presents two mechanistic-empirical methods for bituminous pavement design: the French method (NF P98-086 standard, LCPC-SETRA 1994 handbook, and the Alizé-LCPC software package) and the US method (NCHRP 2004 (MEPDG) guide, AASHTO 2015 manual of practice (MOP), and the AASHTOWare Pavement ME Design (PMED) software package).

The fourth section is dedicated to the comparison of the two methods. Special attention is paid to their differences for taking temperature into account and for the fatigue performance models they present. The equations governing variation in pavement fatigue behaviour in response to temperature will be reviewed. Methods and equations are presented to connect fatigue analysis of each method to the other. The French law of fatigue is expressed in a form ready to insert in the AASHTOWare PMED. The AASHTOWare PMED fatigue prediction procedure is simplified in the form of an aggregated AASHTO pavement fatigue law, which is ready to use with the concept of equivalent temperature.

In sections 5 and 6, the pavement performance predictions made using each method are compared based on experimental data from two sites in France and Québec. The fifth section presents the site, data and analysis for an experimental highway section in Bordeaux, France, while the sixth does so for an experimental section in the province of Québec, Canada. In each case, the available data is specified for: type of structure, tests of bituminous and granular materials, climate, traffic and the applicable performance criteria. This is also the stage at which the climate data files needed for use with the AASHTOWare Pavement ME Design software are prepared.

These two sections set out the main results and the ensuing discussion. The effect of taking actual temperature distributions into account using an incremental calculation of the equivalent temperature under the French method (development in the Alizé-LCPC software) is compared to the US design method (the AASHTOWare Pavement ME Design software). Three climate cases were selected for the comparisons based on temperature effects: one in France (Bordeaux) and two in the United States (Seattle and Phoenix). The results from one experimental site in Québec were also used for comparisons concerning consideration for variations in ground bearing capacity.

The last section contains the conclusions and future prospects.

2. Review of the literature

Recent studies by (Nasimifar et al., 2011), (Rychen, 2013), (Wei et al., 2013), (Wistuba and Walther, 2013), (Bilodeau et al., 2013), (A. Elshaeb et al., 2014), (Saha et al., 2014) (Islam and Tarefder, 2015), (Yang et al., 2015, 2016, 2017), (Hasan et al., 2016), (Hasan and Tarefder, 2017), (Enríquez-de-Salamanca, 2017) (Pereira and Pais, 2017), and (Gudipudi et al., 2017) show that climate conditions have a direct impact on road pavement durability and performance in terms of cracking and permanent deformation.

A state-of-the-art review of current pavement design methods and changes to those methods is presented in the work of (Monismith, 2004), (Dumont and Bressi, 2014) and (Pereira and Pais, 2017). A comparative study of certain pavement design methods, from the point of view of bituminous concrete fatigue, is set out in (Perraton et al., 2019, 2010). Pavement design has evolved over the last few decades, moving from an empirical approach to a mechanistic-empirical approach. The reference for the empirical method in the United States is defined by the American Association of State Highway and Transportation Officials (AASHTO) and described in detail in a design guide (AASHTO, 1993). Its simplicity makes it accessible to a large number of users. However, simplification can be limiting, especially with respect to consideration for climate change (Dumont and Bressi, 2014). The MEPDG (NCHRP, 2004) forms the basis for a new method that is currently under development (AASHTO, 2018), this time using the mechanistic-empirical approach. The new approach (AASHTO, 2015) takes variations in temperature and moisture more explicitly into account when considering the mechanical properties of pavement layers.

Temperature is the climate variable with the most influence over the design of flexible pavement structures (Yang et al., 2016). In France, with respect to the high susceptibility of asphalt mixes to heat, design today relies on a constant "equivalent temperature" (θ_{eq}), generally set at 15 °C (Balay et al., 2012). (Hornych et al., 2013) have determined the actual values of θ_{eq} for various climate conditions, using real-life temperature and traffic measurements on experimental pavements and experimental values for fatigue properties

at various temperatures. The results show significant variation in θ_{eq} with respect to climate and material properties.

There are implications in a context of climate change. A general increase in temperature is forecast in most average air temperature models for 2010 to 2050, and is estimated at 2.2 °C by one of the ten models presented in (Meyer et al., 2014). (Doré et al., 2014) have studied the impact of climate change on pavements in Québec's road network. Climate change can have positive effects (a reduction in frost heave and thermal cracking) and negative effects (an increase in rutting and fatigue cracking) on pavement performance.

3. Mechanistic-empirical methods for bituminous pavement design

Both the French method (LCPC-SETRA, 1994 and standard NF P98-086) and the US method (NCHRP, 2004 and AASHTO, 2015 and 2018) can be classified as mechanistic-empirical approaches, and they are presented in the following pages with a focus on the topic of bottom-up fatigue cracking.

3.1.French pavement design method (NF P98-086)

The rational French method combines a theoretical analysis of pavement mechanics, the results of laboratory modulus and fatigue tests, data from large-scale testing on a circular fatigue test track, and observations from the in-use pavement performance (LCPC-SETRA, 1994). The analysis is based on an isotropic, elastic, multi-layer model (Burmister, 1945), as formulated in the Alizé-LCPC software.

Currently, the method considers variations in the stiffness moduli resulting from the temperature variations to which asphalt mixes are subjected. Heavy vehicle traffic imposes a flexural load that leads to a tensile strain at bottom of the asphalt concrete layers. This tensile strain is calculated at equivalent temperature θ_{eq} , (generally equal to 15 °C in France), and is then compared to the admissible tensile strain $\varepsilon_{t,ad}$ at the same temperature.

The value $\varepsilon_{t,ad}$ is given by (Eq.1):

$$\text{(Eq.1)} \quad \varepsilon_{t,ad} = \varepsilon_6(10^\circ C, 25Hz) \left(\frac{NE}{10^6}\right)^b \left[\frac{E(10^\circ C, 10Hz)}{E(\theta_{eq}, 10Hz)}\right]^n k_c k_r k_s$$

Where:

- $\varepsilon_6(10^\circ C, 25Hz)$: fatigue strain parameter of the bituminous material, representing the tensile strain leading to a lifespan of one million cycles with a probability of failure of 50%, at a temperature of 10 °C and a loading frequency of 25 Hz.
- NE: number of equivalent axles (in terms of material damage) that correspond to the cumulative number (NPL) of heavy vehicles throughout the period under calculation so that $NE = CAM \times NPL$, with CAM being the average coefficient of aggressiveness (or *mean load equivalency factor*) of the traffic.
- E: dynamic modulus of asphalt concrete, according to temperature (10 °C and θ_{eq}) and load frequency. The load frequency is usually set to 10 Hz, but the engineer can adapt this value to specific project needs.
- k_c : calibration coefficient of the design method, used to adjust the predictions produced by laboratory fatigue tests, to the feedback from experimentations done on road networks, test sections and on the LCPC accelerated pavement testing facility (cf. Table 1).
- k_r : risk coefficient according to thickness variation (standard deviation Sh) and dispersion from fatigue tests (standard deviation SN). For example: $k_r = 1$ with a risk calculation of 50%.
- k_s : a reduction factor for the subgrade soil, taking into account the effect of the local load-bearing heterogeneity of a soft layer (cf. Table 2).
- b: slope of the fatigue law of the material ($-1 < b < 0$).
- n: fatigue thermal susceptibility coefficient of the material.

For a given *axle i*, the coefficient of aggressiveness (CA), or *load equivalency factor*, is defined by the $(-1/b)^{th}$ power ratio of its effect, in term of tensile strain, with respect to a reference axle load. As long as the strains are computed with the linear elastic theory, and if there is no change in the tire footprint size and geometry, the CA is exactly the same as the $(-1/b)^{th}$ power ratio of the axial loads (P):

$$\text{(Eq.2)} \quad CA = \left(\frac{\varepsilon_{axle i}}{\varepsilon_{ref}}\right)^{-1/b} = \left(\frac{P_{axle i}}{P_{ref}}\right)^{-1/b}$$

For a given strain level and positive temperatures, (Eq.1) shows that fatigue behaviour is represented by the following law of thermal susceptibility:

$$\text{(Eq.3)} \quad \varepsilon_6(\theta)E(\theta)^n = \text{constant}$$

Where $n = 0.5$ if there are no fatigue test results at various temperatures.

The equivalent temperature θ_{eq} is defined as the constant temperature that leads to the same annual damage as the actual temperature distribution of the site under consideration.

The methodology for calculating the equivalent temperature using the French method is presented in detail in Appendix 6 of the Guide (LCPC–SETRA, 1994) and (Hornych et al., 2013). The equivalent temperature is determined by applying Miner's law (Eq.4), which allows the notion of long-term damage to be introduced (Miner, 1945).

$$\text{(Eq.4)} \quad \sum_i D_i = \sum_i \frac{n_i}{N_i} \leq 1$$

Where:

- D_i : partial damage resulting from the repetition of loads in the incremental analysis period i ,
- n_i : number of loads applied to the pavement during period i .
- N_i : number of admissible loads according to the material fatigue law, under the conditions prevailing during the period i .

Given the expression of the function of the fatigue law, the equivalent temperature is defined implicitly by (Eq.5):

$$\text{(Eq.5)} \quad \frac{1}{N(\theta_{eq})} = \frac{1}{\sum_i n_i(\theta_i)} \left[\sum_{i=1} n_i(\theta_i) \left\{ \frac{\varepsilon_6(\theta_{crit_i})}{\varepsilon_t(P\theta_i(Z))} \right\}^{\frac{1}{b}} \times 10^{-6} \right]$$

Where:

- $N(\theta_{eq})$: the totality of traffic applied at equivalent temperature θ_{eq} ;
- $\varepsilon_6(\theta_i)$: defined above in (Eq.1);

- $\varepsilon_t(\theta_i)$: maximum tensile strain for design purposes of the bituminous pavement layers under the standard design axle (value determined by the structural calculation for the proposed pavement, based on the value of the elasticity moduli of the bituminous layers at temperature θ_i);
- $P\theta_i(Z)$: variable temperature at depth Z that matches the temperature profile of the bituminous layers;
- θ_{criti} : the temperature at the point of application of the fatigue criterion, calculated by considering the spatial average of the temperatures prevailing in a "thin layer" at that level, using the option "subdivision into thin sub-layers" in Alizé-LCPC.

(Eq.5) above, like any other pavement equivalent damage approach, is commonly used over an annual period. However, it can also be used over a period of several years or over the entire pavement design life. Only fatigue damage to the bituminous mixes is considered in (Eq.5), although the design criterion may also be the criterion $\varepsilon_{z,ad}$ for untreated graded aggregate and soil, or even the criterion $\sigma_{t,ad}$ for hydraulic materials (for example mixed and inverted structures).

The deformation of unbound granular materials is verified with respect to the admissible vertical deformation ($\varepsilon_{z,ad}$) calculated using (Eq.6):

$$\text{(Eq.6)} \quad \varepsilon_{z,ad} = A(NE)^{-0.222}$$

- $\varepsilon_{z,ad}$: admissible vertical deformation at the surface of the subgrade soil.
- A: parameter equal to 0.012 for pavements subjected to medium to high traffic ($PL \geq 250,000$) or 0.016 in other cases, with the exception of the granular layers of inverted structures, for which A would be 0.0144.

3.2.US mechanistic-empirical method (AASHTO 2015 and 2018)

As early as 1986, AASHTO recognized the need to move towards a mechanistic-empirical design method that explicitly incorporates the impact of loads and climate on pavement performance. In the wake of the long-term pavement performance (LTPP) monitoring program that began in 1987, the NCHRP 1-37A project was launched in 1998 with funding from AASHTO, the NCHRP and the Federal Highway Administration (FHWA) to develop a more advanced and more comprehensive design guide. The Mechanistic-Empirical

Pavement Design Guide (MEPDG) was published in 2004 (NCHRP, 2004), and then reviewed and revised as part of the NCHRP 1-40A, 1-40B, and 1-40D projects, which led to the development of software released in 2007 under the name DARWin-ME (AASHTO, 2008). The current version (AASHTO 2015 and 2018) is applied using the AASHTOWare Pavement ME Design (PMED) software, renamed in 2013, and updated annually. The distress prediction models are revised and calibrated regularly using data from a large set of actual roadway sections distributed throughout the United States. The primary source of data is the LTPP database, supplemented by data obtained from the MnRoad experiment in Minnesota and other research projects funded, in particular, by the FHWA and various other transportation agencies.

This approach is also based on a structural analysis and the prediction of separate performance indicators, including thermal cracking, fatigue cracking, rutting, and the international roughness index (IRI). The process is illustrated in a simplified way in Figure 1. The approach is iterative and begins with the selection of a given initial structure.

The responses of the road section studied, and the damage incurred, are calculated incrementally during its lifespan. The initial multi-layer structure is subdivided into thinner sub-layers to take into account variations in temperature and loading frequencies in the asphalt layers, and variations in moisture and ice contents in the underlying unbound layers. The subdivision of the multi-layer system into sub-layers is described in Appendix II-1 of the guide (NCHRP, 2004).

- Variations in temperature and moisture in each sub-layer of the pavement structure are calculated hourly using the enhanced integrated climate model (EICM);
- Changes in bituminous viscosity by depth and time result from the Global Aging System model (Mirza and Witczak, 1995) incorporated into the software;
- Traffic loading frequency is adjusted as a function of traffic speed and AC sub-layer depth.
- The critical mechanical responses of the pavement (stresses, strains and displacements) are calculated in terms of isotropic linear elasticity (Burmister, 1945) in each sub-layer using JULEA (Jacob Uzan Layered Elastic Analysis) software incorporated into the AASHTOWare Pavement ME Design software.

The results of these incremental calculations follow the evolution of materials properties during the lifetime of the structure and the elementary damage for each degradation criterion. The cumulative damage is compared to the performance criteria using empirical transfer functions for given levels of statistical reliability. The analysis is repeated until the performance targets for design are met.

The EICM climate model requires the depth of the water table and the entry of hourly climate data for temperature, precipitation, wind speed, percent sunshine and relative humidity. It incorporates three distinct models:

- 1) Climate and material properties;
- 2) Precipitation, infiltration and drainage;
- 3) Frost heave and thaw settlement.

For the US method, the fatigue law is expressed according to (Eq.7):

$$(Eq.7) \quad N_f = C \cdot C_H \cdot \beta_{f1} k_{f1} \left(\frac{1}{\varepsilon_t}\right)^{\beta_{f2} k_{f2}} \left(\frac{1}{145.04 \cdot E}\right)^{\beta_{f3} k_{f3}}$$

Where:

- N_f = admissible number of repetitions;
- ε_t = tensile strain at critical locations (m/m);
- E = dynamic modulus of the bituminous coated material measured in compression, MPa;
- $\beta_{f1} k_{f1}, \beta_{f2} k_{f2}, \beta_{f3} k_{f3}$ = calibration constants;

Version 2.3 of the AASHTOWare PMED software (AASHTO, 2015) incorporated a $\beta_{f1} k_{f1}$ constant (0.007566) from the NCHRP 1-40D project. It was replaced in version 2.5 (AASHTO, 2018) by a coefficient varying from 0.077 to 0.00387 ($\beta_{f1} = 5.014 \cdot (h_{ac}/2.54)^{-3.416}$ and $k_{f1} = 3.75$), for pavement thicknesses (h_{ac}) from 12.7 to 30.5 cm,

respectively. The other constants remained almost identical, with $\beta_{f2}k_{f2} \approx 3.96$ and $\beta_{f3}k_{f3} \approx 1.28$.

$$\text{(Eq.8)} \quad C = 10^{4.84\left(\frac{V_{be}}{V_a+V_{be}}-0.69\right)}$$

V_{be} : Effective binder volume, %

V_a : Voids content, %

For bottom-up (or alligator) cracking, the thickness correction coefficient (C_H) is defined as:

$$\text{(Eq.9)} \quad C_H = \frac{1}{0.000398 + \frac{0.003602}{1 + e^{\left(\frac{11.02 - 3.49 h_{ac}}{2.54}\right)}}$$

Where: h_{ac} total thickness of asphalt mix layers, cm.

This equation gives a C_H value of 250 for all thicknesses greater than 12.5 cm. Damage is calculated taking into account the transversal distribution of trucks within each wheel path. This is achieved by calculating the incremental damage indices on a grid pattern throughout the AC layers at critical depths. The incremental damage index (ΔDI) is calculated by dividing the actual number of axle loads by the allowable number of axle loads (N_f), and referred to as Miner's hypothesis, within a specific time increment and axle-load interval for each axle type. The cumulative damage index (DI) for each critical location is determined by summing the incremental damage indices over time, as shown in (Eq.10):

$$\text{(Eq.10)} \quad DI = \sum (\Delta DI)_{j,m,l,p,T} = \sum \left(\frac{n}{N_f} \right)_{j,m,l,p,T}$$

Where:

- n = Actual number of axle-load applications within a specific time period,
- j = Axle-load interval,
- m = Axle-load type (single, tandem, tridem, or quad),
- l = Type of truck,

- p = Month, and
- T = Median temperature for the five temperature intervals or quintiles used to subdivide each month, Figure 2.

The average (50% risk) area of alligator cracking, expressed as a percentage of the total lane area, is calculated empirically:

$$\text{(Eq.11)} \quad \overline{FC} = \left(\frac{1}{60}\right) \left(\frac{C_4}{1+e^{(C_1 C_1^* + C_2 C_2^* \text{Log}(100 \cdot \text{DI}))}}\right)$$

It is important to note that the US national calibrating constants were modified in version 2.5 (AASHTO, 2018) and that coefficients C_2 , C_2^* and C_1^* are a function of total AC thickness: $C_1 = 1.31$; $C_2 = 0.867 + 0.2583(h_{ac}/2.54)$ with limits for h_{ac} between 12.7 and 30.48 cm; $C_4 = 6000$; $C_2^* = -2.40874 - 39.748(1 + h_{ac}/2.54)^{-2.856}$; $C_1^* = -2 C_2^*$. Previously, this equation resulted in a 50% cracking of the lane area at a damage of 100% (DI), which is no longer the case in the current version.

The US method includes the notion of statistical reliability ($R = 1 - \text{risk}$) by adding the product of the reduced centered variable from the standard probability distribution ($Zr < 0$) with the standard deviation of the residual errors (se), to the average predicted area of fatigue cracking (Eq.12). The standard deviation of the residual errors is a function of the average predicted area of fatigue cracking (Eq.13):

$$\text{(Eq.12)} \quad FC = \overline{FC} - Zr \cdot se$$

$$\text{(Eq.13)} \quad se = 1.13 + \frac{13}{1+e^{(7.57-15.5 \text{Log}(\overline{FC}+0.0001))}}$$

(Eq.7) results historically from the fatigue formula developed by the Asphalt Institute from data on four-point bending tests with controlled stress. It was calibrated by (Finn et al., 1977) based on the results of the AASHO road test. (Copper and Pell, 1974) proposed (Eq.8) to include the correction factor (C) taking into account the proportions by volume of the mix. The equation was revised by (El-Basyouny and Witczak, 2005) based on data from the US long-term pavement performance (LTPP) program. The thickness correction coefficient (C_H) was developed specifically for the MEPDG, as part of the NCHRP 1-37A research program. The US method also includes a separate model for top-down fatigue

cracking. The calibration of these two separate models is hampered by difficulties to differentiate on site between bottom-up and top-down cracking.

4. Comparison and correspondence of the two methods

Table 3 summarizes the differences between the French (Alizé-LCPC software) and US (AASHTOWare Pavement ME Design software) flexible pavement design methods. It is important to note that the US method introduces several additional degradation mechanisms (top-down cracking, thermal cracking, international roughness index (IRI)), a more elaborate empirical rutting model, and a more detailed breakdown of traffic and climate variations.

The structural calculations have at least two obvious differences. The concepts of equivalent single axle loads (ESALs) and equivalent temperature (θ_{eq}), which are used in the French method, are not used in the US method. In both cases damages are calculated using Miner's law, but it is a separate, optional process in the French method. ESALs and equivalent temperature aggregations reduce the computational cost of the French method. On the other hand, the disaggregated steps of the US method make room for additional features.

Also, the French method does not consider seasonal variations in ground bearing capacity at all, and the US method introduces a binder aging model. The main differences, and the keys to their correspondence, are studied in the following subsections with a focus on issues relevant to bottom-up fatigue prediction.

4.1. Correspondence of traffic inputs

The design concept of the equivalent single axle load (ESAL) is a legacy of the AASHO Road Test. ESALs of 80 kN and their corresponding load equivalency factors are still used today as indicated in the 1993 AASHTO Guide. The French method uses the same concept with a reference twin tires/single axle load of 130 kN. The load footprint illustrated in Table 4 is represented by two discs with a radius of 125 mm at a distance of 375 mm, exercising a uniform pressure of 662 kPa. Table 4 also describes the 80 kN load used for

the SERUL site in Québec. The dual tire spacing (305 mm) and the tire pressure (827.4 kPa) values have been chosen according to the default values in AASHTOWare PMED.

The AASHTOWare PMED software does not use the concept of ESAL, meaning that it does not require the development of load equivalency factors. Instead, the full distribution of axle loads for each type of axle must be entered.

As explained earlier in (Eq.2), this difference by itself is expected to have limited or negligible impacts on the pavement fatigue results. To get the correspondence, we chose to enter a traffic load expressed solely in terms of the reference axles defined in Table 4, for the sites in France and Québec respectively. In this way, the simulated traffic comprises 100% trucks with two single axles (class 5), with 100% of the axles entered in the load group corresponding to the reference load. The operational speed was set at 80 km/h in all cases.

4.2. Rheological models for bitumen

The effective bitumen volume in the mix, the air void percentage, and the data for the complex moduli of the bitumen and mix, are used as inputs for the AASHTOWare PMED software. For bitumen, the level 1 standard for the complex shear modulus $|G^*|$ and phase angle (δ) are given at a frequency of 1.59 Hz ($\omega = 10$ rad/s) and a range of temperatures (4.5 to 54 °C). The program first converts the binder stiffness data at each temperature to viscosity using an empirical equation (Eq.14). The parameters of the A-VTS equation (Eq.15) are then found by linear regression after log-log transformation of the viscosity data and log transformation of the temperature data.

$$\text{(Eq.14)} \quad \eta = 1000 \frac{|G^*|}{\omega} \left(\frac{1}{\sin \delta} \right)^{4.8628}$$

$$\text{(Eq.15)} \quad \log \log \eta = A + VTS \log(T_K \times 9/5)$$

Where:

- $|G^*|$ = binder complex shear modulus (Pa)
- δ = binder phase angle (degrees)

- φ = standard frequency (10 rad/s)
- T_K = temperature at which the viscosity was estimated (Kelvin)
- η = viscosity (centipoise)
- A , VTS = regression parameters

A more extensive description of the viscoelastic behaviour of bitumen can be represented using the "Huet-Such" rheological model (Such, 1983). The diagram and equations for the "Huet-Such" model are presented in Figure 3. Visco-Analysis Software (Chailleux, 2007) was used to adjust the model with the experimental data. The temperature translations were carried out using the τ parameter from the WLF law (Williams et al., 1955).

The results from the complex modulus testing of the bitumen used on express highway A63 and the SERUL site, described next, are presented in Figure 4 as (a) and (b) respectively. This involves recalculating bitumen shear module and phase angle values from experimental measurements for different temperatures (from 10 to 50 °C) at the frequency of 1.59Hz, applying the time–temperature superposition principle and the Huet-Such model. For the PG 58-34 bitumen (SERUL), cross-testing was carried out by the laboratory run in France by the division "Matériaux pour Infrastructures de Transport" (MIT/IFSTTAR) and the laboratory of the ministère des Transports du Québec (MTQ), respectively using Métravib and DSR (AASHTO T315). Experimental data has been fitted by the Huet-Such rheological model and the 9 parameters (G_∞ , δ , k , h , β , τ_0 , A_0 , A_1 and A_2) obtained are shown in Table 5.

It is important to note that the AASHTOWare software does not recognize the parameters of the modified Huet-Such model, but rather a table of values at various temperatures, and it was observed that the DSR values determined for a reduced range of 20 to 50 °C did not lead to the expected results. Because it is important to cover the entire range recommended in the guide (NCHRP, 2004), from 4.5 to 54 °C, the Métravib results were selected, since they were the only results that covered the whole range of temperatures. The A-VTS regression parameters, as reported by the AASHTOWare are shown in Table 5.

4.3. AC dynamic modulus

The AC dynamic modulus is basically a function of time and temperature. It decreases when the temperature or time of loading increases. Pavement design methods typically convert time of loading into frequency ($f = 1/t$).

For this purpose, the bitumen mix courses in AASHTOWare PMED are subdivided into sub-layers, and their dynamic modulus is modeled according to the following sigmoidal function:

$$\text{(Eq.16)} \quad \log(145.0377 \cdot E) = \delta + \frac{\alpha}{1 + e^{\beta + \gamma \cdot \log(t_r)}}$$

Where:

- $\delta, \alpha, \beta, \gamma$ = material constants
- t_r = time of loading at the reference temperature, determined with:
$$\log(t_r) = \log(1/f) - c(\log(\eta) - \log(\eta_{T_R}))$$
- c = shift factor describing the temperature dependency of the modulus
- f = loading frequency (Hz)
- η = binder viscosity at any temperature and aging level, cf. (Eq.15)
- η_{T_R} = binder viscosity at reference temperature (21.1 °C) (centipoise)

The NCHRP (Appendix CC-3) describes the US method to compute the loading frequency as a function of traffic speed and sub-layer depth. It assumes a stress envelope spreading at 45° after transformation with the method of equivalent thicknesses. According to Table 6, the load frequency may range from 95 to 10 Hz for an operational speed between 70 and 100 km/h and depths between 12.5 and 190 mm. The near-surface sub-layer moduli are then expected to be higher than the 10 Hz modulus value typically used in the French method.

Furthermore, the AASHTOWare PMED software uses a bitumen aging gradient to assess the increase over time of binder viscosity and modulus of the bituminous mix. This empirical formula, known as the Global Aging System, is described in (NCHRP, 2004). The equations are a function of the mean annual air temperature (MAAT), the sub-layer depth, the age in months, and the binder and mix properties.

The software then calculates the internal temperature, load frequency, aging factor and modulus of each sub-layer in relation to external traffic and climate factors. An example of modulus values at different depths and over the pavement design period (20 years) is shown in Figure 5, after simplifying for a constant temperature of 15 °C. The figure is normalized by dividing by the modulus E (15 °C, 10 Hz) used in the French method, which is 7000 MPa and 9000 MPa for the BBSG 3 and GB 3 mixes respectively. All the curves include the simultaneous effects of aging and load frequency. Equivalent curves combining the sub-layers in complete layers are also illustrated according to the following weighted average equation, based on the method of equivalent thicknesses.

$$\text{(Eq.17)} \quad E_{eq} = \left(\frac{\sum h_i \times \sqrt[3]{E_i}}{\sum h_i} \right)^3$$

This idea of aging corresponds with observations made at the MIT/IFSTTAR laboratory (cf. Table 7). (Marsac, 2018) has assessed the effect of aging using modulus tests and fatigue tests at 24-year intervals on a gravel/bitumen (GB) mix and high modulus asphalt (EME). These results show that the aging of the bituminous binder significantly increases the dynamic modulus of the asphalt (+36 to 65% for GB). The data also shows that the long term aging significantly increases the slope (-1/b) of the fatigue curve (+93% for GB). This has the effect of accelerating or slowing damage from fatigue, depending on the pavement loading conditions (Marsac, 2018).

The change in the slope of the fatigue curve is not taken into account, but the US method is the only one that simulates the long-term increase of modulus. Figure 5 shows that the same set of laboratory data involve significantly higher modulus values. This must be taken into account when transferring the pavement performance model from one method to the other. For this purpose, the following may apply:

- When using the AASHTO fatigue law in any layered elastic analysis software, moduli can be based on the equivalent temperature θ_{eq2} , defined as the constant temperature that leads to the same total damage as the actual AASHTOare moduli distribution for the whole design period of the site under consideration. The AASHTOare provides a convenient intermediate output file (_modulus.tmp)

listing the results of the modulus, Poisson ratio, temperature and frequency for each sub-layer and monthly quintile. The equivalent temperature θ_{eq2} can be computed with (Eq.5) from these sets of moduli.

- When using the LCPC fatigue law in any layered elastic analysis software, the moduli need to be the same $E(\theta_{eq}, 10Hz)$ as those used in the French design method. This can be done in AASHTOWare PMED with the level 1 dynamic modulus input, repeating the same modulus value at each temperature and load frequency. In this case, the (Eq.16) converges to $\alpha = 0$, $\delta = \log(145.0377 \cdot E)$ and reverts to $E = 10^\delta / 145.0377$, independently from traffic speed, aging and other climatic inputs.

4.4. Correspondence of fatigue equations

Both methods take into account the total thickness of the bituminous mix (h_{ac}) using layered linear elastic analysis (Burmister, 1945) for the computation of the tensile strain (ε_t). However, the US method uses the AC thickness in the calculation of several empirical calibration constants (β_{f1} , C_H and \overline{FC}).

The French method considers that the pavement reaches the end of its life when the Miner's damage ratio reaches 100%, while the US method may consider a different ratio because of the calibration constants, cracking threshold and level of reliability used in (Eq.11) to (Eq.13). For this reason, it would not be appropriate to compare (Eq.7) directly with (Eq.1).

It is more appropriate to make a comparison using all the elements present in each design method. The simplifications inherent in the French method guide the choice of certain common denominators: a constant equivalent temperature (θ_{eq}), a constant modulus for unbound materials, a single configuration for traffic loads (equivalent single axle loads, or ESALs), an implicit traffic wander standard deviation of 220 mm (included in the calibration coefficient k_c), an implicit fatigue cracking threshold (50%), and an implicit rutting depth (20 mm). The comparison must also be based on the same risk or reliability level.

It is possible to write an "aggregated AASHTO" pavement fatigue law for use within the aggregated framework of the French method, based on the concept equivalent temperature:

$$(Eq.18) \quad \varepsilon_{t,ad} = \left(\frac{DI \cdot TWF \cdot C \cdot C_H \cdot \beta_{f1} k_{f1}}{N_f (145.0377 \cdot E)^{\beta_3 k_3}} \right)^{\frac{1}{\beta_{f2} k_{f2}}}$$

The formula is based on (Eq.7), but isolates tensile strain (ε_t in m/m) and introduces the factors DI, and TWF. The damage index ($DI = f(FC, h_{ac}, Z_r, se)$) corresponds to the cracking threshold and level of reliability used. It is determined by inverting (Eq.11), combined with (Eq.13) and (Eq.12). The damage index must, however, be determined numerically, for example using the secant method, given that (Eq.13) expresses the standard error (se) as a function of \overline{FC} rather than FC.

The traffic wandering factor TWF is introduced to handle the effect of traffic wander. In this connection a series of simulations was conducted with the AASHTOWare PMED software to obtain the relation between the damage ratio and the traffic wander standard deviation (Figure 6). We can deduct from this that the traffic wander of 220 mm assumed in the French method corresponds to a TWF of 1.29.

The "aggregated AASHTO" pavement fatigue law (Eq.18) is graphed in Figure 7 alongside the (LCPC-SETRA 1994) law, for various pavement thicknesses and in light of the design parameters given in the next sections. It shows that, for the cases under examination, both laws of fatigue tend to resemble each other for thicker pavement layers (20-25 cm or more) and depending on the number of cycles N_f considered. However, it can be seen that the AASHTO fatigue law becomes a lot more permissive as the pavement thickness decreases.

In the case of the AASHTOWare PMED software, the laws of fatigue must be expressed in the form shown by (Eq.7). The equations (Eq.19), (Eq.20) and (Eq.21) make it possible to inject the laws of fatigue of the French method (Eq.1), in order to neutralize the effect of (Eq.8) to (Eq.12).

$$(Eq.19) \quad \beta_{f1} k_{f1} = \frac{(\varepsilon_6 k_c k_r k_s)^{-1/b} \cdot (145.0377 \cdot E(10^0 C))^{-n/b} \cdot 10^6}{C \cdot C_H \cdot DI \cdot TWF} \quad (\text{with } \varepsilon_6 \text{ in m/m and E in MPa})$$

$$\text{(Eq.20)} \quad \beta_{f2} k_{f2} = \frac{-1}{b}$$

$$\text{(Eq.21)} \quad \beta_{f3} k_{f3} = \frac{-n}{b}$$

4.5. Effect of temperature on bituminous mix fatigue

Fatigue tests can be carried out on asphalt mixes using homogeneous (tension-compression) or non-homogenous (two-, three- or four-point bending and indirect tensile) stress states (AAPT, 2016). Both the French and US standards are based on the non-homogenous test. In France, the two-point bending test, on trapezoidal beam specimens, is used (NF EN 12697-24(Appendix A)). In the United States, the four-point bending (4PB) test is standardized as testing method AASHTO T 321.¹

Fatigue is generally recognized as a relatively complex failure mechanism that includes the initiation and the spread of cracking, the end of cracking and self-repair phenomena. In addition, current fatigue tests on asphalt mixes are hard to correlate, whether between tests methods or with in-situ performance.

According to (Eq.1) and (Eq.7), the two design methods consider that an increase in temperature enhances the fatigue performance of bituminous mixes, under a given strain level. However the temperature relationship maybe more complicated.

Numerous studies have examined the effect of temperature on the fatigue behaviour of asphalt mixes using two-point bending tests (Moutier, 1991); (Domec, 2005); (Domec et al., 2005); (Bodin et al., 2010); (Marsac et al., 2010); four-point bending tests (Francken and Verstraeten, 1994); (Tayebali et al., 1994); (Doucet, 1999); (de Mello et al., 2016), and tension-compression tests (Lundstrom et al., 2004); (Touhara, 2012). Results are illustrated in Figure 8 (normalized to 10 °C) next to the French law of thermal susceptibility (Eq.3).

¹ AASHTO T 321: Determining the Fatigue Life of Compacted Hot-Mix Asphalt (HMA) Subjected to Repeated Flexural Bending.

Most of them indicate a non-linear trend similar to a parabolic curve with a minimum around 5 to 10 °C. The results from (Tayebali et al., 1994), although not parabolic, indicate an increase in the slope of the Wöhler curve at low temperature.

The Alizé-LCPC software was modified (research version) to include the equations that describe these parabolic curves. The results can be used to assess the effect of the fatigue law on the equivalent temperature calculation, compared to the other laws in the library, and then to study the repercussions on the calculation of lifespan using the French method.

5. Express highway A63 (Bordeaux, France)

The road section studied in France is part of express highway A63 near the city of Bordeaux. The present section presents the inputs, followed by analysis and results.

5.1. Climate

Hourly temperature data by depth are available over a 10-year period, from August 1, 2003 to August 1, 2013 (from the Begles station near Bordeaux). One example of temperature data from 2006 is presented in Figure 9 for the 7 sensors up to 1 metre in depth. The data can be used to calculate the equivalent temperature for the French method (section 5.1.1). The site is characterized by an annual variation in air temperature of -8 to 39 °C, in surface temperature of -12 to 52 °C, and in base course temperature of -3 to 34 °C. The variation ranges at various depths are shown in Table 8.

Atmospheric data (air temperature, precipitation, wind speed, percent sunshine, relative humidity), on a daily basis from 2003 to 2016, have been provided by Météo France for the Bordeaux-Merignac weather station (latitude 44°49'48"N, longitude 0°41'24"W). The data were entered into a file in ".hcd" format compatible with the AASHTOWare PMED software (cf. Figure 10). The mean annual air temperature (MAAT) is 13.8 °C, and the mean annual precipitation is 840 mm.

5.2. Additional climate scenarios

To assess the effect of climate conditions more extensively, two other sets of climate data were selected from among those available in the AASHTOWare PMED software package

for the United States. The first set is from the colder climate of Seattle in the State of Washington, with a mean annual air temperature of 10 °C (NARR data from 1979-01-01 to 2015-06-30 in file 24233.hcd), while the second is from the warmer climate of Phoenix, Arizona, with a mean annual air temperature of 24 °C (NARR data from 1979-01-01 to 2015-06-30 in file 23183.hcd). The temperature distribution in the pavement layers is needed to calculate the equivalent temperature for the French method. The temperatures generated by the EICM component of the AASHTOWare PMED software were selected. Seattle and Phoenix are wet and dry climates with mean annual precipitations of 1170 mm and 252 mm respectively.

Many other analyses based on equivalent temperatures ranging from 0 to 40 °C have been added. Figuring out how to adapt them for the AASHTOWare PMED was challenging. In order to achieve this, two distinct approaches have been experimented.

An arbitrary “.hcd” climatic file (Bordeaux, Seattle and Phoenix) was used as template for the first approach. The net short wave radiation (Q_s), net long wave radiation (Q_l) and convection heat transfer (Q_c) parameters were removed in order to obtain constant temperatures. Short wave radiation was removed by setting AC surface shortwave absorptivity to zero instead of the default value of 0.85. Long wave radiation was minimized by setting sunshine to zero. Convection heat transfer was removed by setting wind speed to zero, although this was not necessary since difference between air and surface temperatures had already been eliminated. The combination of these parameters has been verified to produce a constant asphalt temperature as desired. Inside the range of the climate files analysed, the effects of precipitation, relative humidity and depth of water table (2 to 15 m) were found to be negligible on the pavement performance predicted for the same temperature conditions. After this verification, the depth of the water table was always set at 2 m.

Figure 5 is based on this method. However, this involves an equivalent temperature θ_{eq} identical to the mean air temperature (MAAT), which is an important input to the Global Aging System. These two values are not identical in practice, making simulations unrealistic. This approach also implies that dynamic moduli are incompatible with the calibration of the French fatigue law due to aging and load frequency considerations.

The second approach consists in using the equivalent temperature θ_{eq} (and θ_{eq2} as needed), to determine the constant layers moduli to input into the software. This approach, which is explained in section 4.3, is more in line with the theory underlying the two design methods. This approach has been verified to produce a constant asphalt modulus as desired, without the shortcomings of the first approach. Results from this method will be compared with those from the detailed climatic data.

5.3. Traffic and level of reliability

The thickness of the AC base course (GB 3) of express highway A63 (Figure 11) was redesigned for the Bordeaux climate, based on an annual daily traffic average of 2,000 heavy trucks per day in the busiest lane, and a *load equivalency factor* of 0.8 (NF P98-086, information appendix C). Over 20 years, with an arithmetic increase rate of 3%, this corresponds to cumulative heavy vehicle traffic of 15 million equivalent single axle loads (ESALS₁₃₀).

According to standard NF P98-086 (information appendix E), for express highways pavements with class Ts traffic (average annual daily traffic of 2,000 to 5,000 vehicles), a risk coefficient of 1% is selected ($k_r = 0.658$). This is equivalent to a reliability level of 99% ($Z_r = u = -2.327$).

5.4. Pavement structure and materials

The thick bituminous pavement (cf. Figure 11) comprises three hot mix AC layers: one 8 cm surface course of semi-coarse asphalt (*béton bitumineux semi-grenu*, or BBSG), and two courses (base and foundation) of a gravel/bitumen mix (*grave bitume*, or GB) mix, each 13 cm thick. The surface course is formulated with 5.3 ppc grade 35/50 pure bitumen ($V_{be} = 11.9\%$, $V_a = 5.2\%$), while the gravel/bitumen mix uses the same bitumen at 4.3 ppc ($V_{be} = 10.79\%$, $V_a = 9\%$). This design, giving a total AC thickness of 34 cm, is found in the catalogue (LCPC-SETRA, 1998). The bituminous mixes are laid on a Type PF3 working platform with a constant modulus (E) of 120 MPa. This platform consists of a granular base of untreated gravel over natural gravel.

Complex modulus testing has been done on the two bituminous mixes. The results of the two-point bending fatigue test on the GB 3 foundation course are presented in (Bodin et al., 2010). The standard parameters for design using the Alizé-LCPC software are presented in Table 9 (French standard NF P98-086 – Appendix F). The results from the testing of the complex modulus for bitumen (Table 5) and bituminous mixes are also entered into the AASHTOWare PMED software for various frequencies and temperatures. Table 10 presents the coefficients of (Eq.16) as reported by the software, with the corresponding statistical regression indicators of precision (SSE and Sy/Se).

5.5.Results using the French approach

Using the French method, design is based on an equivalent temperature θ_{eq} , defined as the constant temperature that results in the same damage as the actual temperature distribution (Eq.5). The effect of the fatigue law and the choice of time increment are examined here.

Table 11 presents the θ_{eq} results for three years under the climate of Bordeaux (2004, 2006 and 2008). Results range from 15.4 to 20.8 °C. The differences obtained by varying the time increment (hourly, daily, weekly and monthly) are typically less than 1 °C, except for ESG 14 in the year 2004 where the difference was 1.7 °C. However, differences of up to 4.2 °C are obtained by varying the fatigue law. The choice of the reference year leads to differences from 0.7 to 1.7 °C, depending on the fatigue law. Based on the results in Table 11, the equivalent temperature for the Bordeaux site is around 19 °C, for the law (LCPC-SETRA, 1994), or a little more than 5 °C above the mean annual air temperature of 13.8 °C.

Table 12(a) presents the θ_{eq} computed from the asphalt temperatures reported in the AASHTOWare PMED's “_modulus.tmp” intermediate results file for Seattle, Bordeaux and Phoenix. The mid-quintile result for Bordeaux ($\theta_{eq} = 19.6$ °C) is similar to those from Table 11 with the LCPC-SETRA fatigue law, and the results for Seattle (15.0 °C) and Phoenix (29.1 °C) are also higher than the MAAT by about 5 °C. Results using all quintiles tend to be a little higher. Table 12(b) presents the θ_{eq2} computed from the asphalt moduli reported in the same intermediate results file. These values fall between the MAAT and θ_{eq} .

A calculation is carried out with layered elastic analysis to determine the pavement lifespan of the initial pavement structure and to optimize the thicknesses of the AC base course as a function of the equivalent temperature. The results for various θ_{eq} from 5 to 40 °C are shown in Table 13. The increase in θ_{eq} leads to a reduction in lifespan, which in turn points to the need to increase the thickness of the GB 3 base course compared to the reference case of 15 °C. It appears that an increase of 1 °C leads to a reduction of 8% in the pavement lifespan and an increase of 0.5 cm in the required thickness.

5.6. Results using the AASHTOWare PMED

The pavement performance and design calculations were also conducted using the AASHTOWare Pavement ME Design software (version 2.5.5). To compare results with the French method, the seasonal variations of unbound granular and soils layers moduli were deactivated in AASHTOWare by setting a subgrade annual constant moduli (120 MPa).

The AASHTOWare PMED also used the climate data to simulate the changes in the modulus of the bituminous sub-layers throughout the 20-year analysis period. These are illustrated in Figure 5, under a constant temperature of 15 °C, and in Figure 12 with the climatic data from Bordeaux. Values in Figure 12 are aggregated in the θ_{eq2} reported in Table 12(b). These include the temperature as well as material, aging and traffic load frequency effects.

The fatigue cracking was calculated for the US and French laws of fatigue (presented above in sections 3 and 4.4). Table 14 groups the specific parameters of the fatigue models that were plotted in Figure 7 and entered into the AASHTOWare PMED software. Coefficients $\beta_{f1}k_{f1}$ needed some work to be determined for the French fatigue law. After the numerical resolution of the damage index (DI), results from (Eq.19) were reduced to a quadratic regression equation that made it possible to approach the results with an R^2 coefficient over 0.99998 for any thicknesses (h_{ac}) between 12.7 and 30.5 cm. For highway A63, the thresholds used for fatigue cracking (FC) and rutting depth are 50% and 20 mm.

The results with the French LCPC-SETRA fatigue law are appended at bottom of Table 13, under those of the French method for each equivalent temperature. The results with the US AASHTO 2018 fatigue law are shown in Table 15, and represent the US method for the three detailed .hcd climate files (Seattle, Bordeaux and Phoenix).

Table 15(a) presents the anticipated degradation while Table 15(b) shows the useful life of the pavement before the indicated threshold is reached. It can be observed that the AASHTOWare PMED software predicts more structural degradations with an increase in temperature.

In addition, the software predicts more thermal cracking in the warmer climate of Phoenix, which is counter-intuitive and may be subject to caution. This result can be explained by a discontinuity in the calibration of the software, which selects another formula for thermal cracking when the mean annual air temperature is higher than 13.89 °C.

A design calculation is carried out to optimize the thicknesses of the AC base course for the three climate files. The results are shown in Table 15(c). Warmer climate leads to a reduction in lifespan, which in turn points to the need to increase the thickness.

Results for bottom-up fatigue cracking, using in AASHTOWare PMED the constant moduli corresponding to θ_{eq2} , are presented in Table 15 (a, b and c) under the results obtained from the detailed analysis of hourly temperatures. The similarity of the results shows the efficiency of θ_{eq2} as a single parameter equivalent to thousands of damage computations.

5.7.Results from the aggregated AASHTO pavement fatigue law

As defined earlier, θ_{eq2} from Table 12 indicates the moduli to use with the aggregated AASHTO 2018 pavement fatigue law (Eq.18), integrating the effects of aging and load frequency in the bituminous sub-layers. Table 16 presents these moduli and the results obtained with this method in terms of lifespan and design thickness.

5.8. Comparison and discussion of the results for express highway A63

A comparative summary is presented in Table 17 and illustrated in Figure 13 as a function of θ_{eq} . The results for bottom-up fatigue cracking can be compared in terms of lifespan for the structure in place as well as in terms of the minimum thickness needed to get a service life of 20 years.

The results from the US method (AASHTO fatigue law) appear more sensitive to the equivalent temperature. For this particular case, the results from both methods are nearly identical for the climate of Seattle (23.4 vs 22.9 years and 25.2 vs 25.0 cm) and increasingly different for Bordeaux (16.6 vs 13.8 years and 27 vs 28.6 cm) and Phoenix (6.8 vs 3.8 years and 31.9 vs 38.0 cm).

In the Phoenix case, the absolute difference in lifespan is not significantly higher than for Bordeaux (3.0 vs 2.8 years), but the relative difference is higher. This case, however, is atypical as pavement designs are rarely, if ever, created for such a short service life. In Phoenix, the warmer temperatures decrease the asphalt modulus, which in turns increase the thickness needed to compensate for the difference in lifespan.

A comparison is also made between the two hybrid methods, applying the French fatigue law in the US AASHTO Ware PMED and applying the aggregated AASHTO fatigue law with the concept of equivalent temperature. The results from both hybrid methods are practically the same as the results from the original French and US design methods.

Based on these results, it is clear that the fatigue law and temperature are key parameters with the two mechanistic-empirical pavement design methods. The thermo-sensitive behaviour of bituminous mixes reduces the high-temperature modulus, which increases strain and damage from fatigue. This results in an increase in the thickness of the asphalt needed to support traffic loads. The results concord with the results obtained by (Silva et al., 2008) based on the fatigue equation produced by the Shell international petroleum company.

The behaviour of AC interlayers interface bonding in response to temperature is another important parameter. The work of (Diakhaté et al., 2011) shows a drastic reduction in

bonding strength with an increase in temperature. However, in this study only the hypothesis of a bonded interface was taken into account.

6. Montmorency Forest (SERUL, Québec)

The second road section studied is part of the experimental road site operated by Université Laval (known as the "SERUL" site), in the Montmorency Forest about 70 km north of Québec City (Badiane, 2016).

6.1. Climate (Montmorency Forest)

A road weather monitoring station is present at the SERUL site, equipped with a 3 m soil temperature probe (18 thermistors). Daily temperature data (November 2010 to June 2017) was also recorded at the weather station in "Parc national de la Jacques-Cartier" at 17 depths from 5 cm to 3 m. The records show an annual variation in air temperature of -30 °C to 23 °C (Table 18). The variation is reduced to -11 °C to 21 °C at a depth of 90 cm and 0 °C to 12 °C at a depth of 3m.

Hourly weather data was extracted from the Environment Canada site (Canada, 2011) for January 1, 2008 to December 31, 2016. The data from the weather station FORET MONTMORENCY RCS (latitude 47°19'22"N, longitude 71°08'54"W and altitude 672.8 m) included the temperature, wind speed and relative humidity, at hourly intervals. However, precipitation was available at daily intervals only and was evenly distributed over each 24-hour interval. The missing data was compiled from the closest stations within a 50 km radius. Sunshine data was completed using data from Québec City, available in the library for the AASHTOWare PMED software. A new ".hcd" file was prepared using all this data (Figure 14). The mean annual air temperature (MAAT) is 1.8 °C, the mean annual precipitation is about 1400 mm and the freezing index is 1560 °C-days.

6.2. Structure and materials

The structural design, Figure 15, was verified using both mechanistic-empirical methods (French and US). This thick bituminous pavement (total hot mix AC thickness of 20 cm) is made up of two layers of medium-coarse asphalt (*enrobé semi-grenu* or ESG 10), each

5 cm thick, and a 10 cm base layer of gravel/bitumen (GB 20). All these bituminous mixes were made using grade PG 58-34 bitumen. Complex modulus testing of the bitumen was conducted and is described in section 4.2 (cf. Table 5). The mix formulas specified an effective binder volume (V_{be}) of 12.2% and 10.2% for bituminous mixes ESG 10 and GB 20, respectively. The void percentages (V_a) for the two bituminous mixes were 3.4% and 5.8% on average on the test strip. The pavement is laid over a 0-20 mm granular base material (MG 20), 20 cm thick, and a subbase of sand (MG 112, with 72% and 5% passing sieves of 5 mm and 80 μ m respectively), 45 cm thick, and a natural subgrade soil of silty sand (unified soil classification SM, with 21% of fines passing an 80 μ m sieve).

Complex modulus test results have been published by (Badiane, 2016) and fatigue test results from similar AC mixes have been published by (Doucet, 1999). The standard parameters used in the Alizé-LCPC software are presented in Table 9, and the corresponding AASHTOWare dynamic modulus parameters are indicated in Table 10. The value of ϵ_6 (10 °C, 25 Hz) for GB 20 is 186 μ def, measured using a four-point bending test. This value is high compared to the usual values in France. According to (Di Benedetto et al., 2004), for non-homogeneous tests, not only the type of test but also the size of sample shows pronounced influence.

The French model and its calibration in particular, are based on a two-point bending test for fatigue. A reduction must be applied to the value obtained to enter it in the French design method. The reduction is made by setting the value of k_c at 1 instead of 1.3 to take the high ϵ_6 value into account. The resilient moduli used for the unbound base, subbase and subgrade layers (250, 109 and 54 MPa, respectively) were determined through FWD (falling weight deflectometer) testing and resilient moduli testing in the laboratory (testing methods LC 22-400 and AASHTO T307-99).

These inputs were used to study the effect of modulus variation on various layers, as a function of temperature and moisture, on pavement structural performance.

6.3. Traffic and level of reliability

For the standards in force in Québec, the software Chaussée 2, based on the empirical method (AASHTO, 1993), indicates that the pavement structure at the SERUL site (Figure

15) can support a cumulative traffic load of 23.5 million ESALs₈₀ before reaching a loss of viability index (Δ PSI) of 2.0, with a reliability level of 80% (the criterion for a regional road; $Z_r = u = -0.841$). This result is used as traffic and reliability inputs for the following performance predictions.

6.4. Equivalent temperatures

Equivalent temperature, as it is understood in the French method (Eq.5), can be calculated for the SERUL site using the daily temperature measurements for the pavement. As 22% of data is missing for sensors in bituminous mixes, a synthetic year was produced by averaging the data available for each of the 365 days of the year. The results, presented in Table 19(a), show an equivalent temperature of 11.3 and 12.5 °C respectively, depending on the fatigue law.

The equivalent temperature θ_{eq} was also calculated from the temperatures generated by the AASHTOWare enhanced integrated climatic model (EICM) based on air temperatures for the 20-year design period. These results, shown in Table 19(b), are slightly lower (9.6 and 10.6 °C). The table also shows the θ_{eq2} (4.7 °C) calculated from the layer moduli generated by the AASHTOWare, including use of the aging and traffic loading frequency models underlying its calibration.

For comparison purposes, another set of equivalent temperatures was added in the same table, using the seasonal variation of the unbound layers moduli option available in the AASHTOWare PMED software. These modulus simulations are illustrated in Figure 16 (a) and (b) respectively. Roy et al. (1997) presented a method to integrate such variations with the equivalent damage approach, also based on Miner's Law and applicable to the definition of equivalent temperature. This leads to a small increase in θ_{eq} and θ_{eq2} attributable to additional structural damage due to weakening caused by the spring thaw.

6.5. Verification of the structure at the SERUL site using the concept of equivalent temperature

All the results of fatigue cracking analysis based on equivalent temperature are presented in Table 20. A first design calculation ($\theta_{eq} = 11.3$ °C, $E_{\theta} = 7930$ and 9270 MPa, $\varepsilon_6 = 186$ $\mu\varepsilon$, $-1/b=5$, $n=0.5$, $k_r = 0.859$, $k_c = 1$, $k_s = 1/1.1$) shows that the pavement meets the traffic and failure criteria in the Alizé-LCPC software for fatigue cracking ($\varepsilon_{t\ calc} = 71.6$ $\mu\text{def} < \varepsilon_{t\ admis} = 80.0$ μdef) and for rutting of the subgrade soil ($\varepsilon_{z\ calc} = 146.0$ $\mu\text{def} \ll \varepsilon_{z\ admis} = 369.8$ μdef). This design model allows a minimum total thickness of 18.4 cm of asphalt (8.4 cm ESG 10 + 10 cm GB 20)² for the 20-year design period. The application of all the coefficients measured in the laboratory (Doucet 1999: $\theta_{eq} = 12.5$ °C, $-1/b = 4.23$ and $n = 0.3806$) would, otherwise, require a minimum asphalt thickness of 20.6 cm ($\varepsilon_{t\ admis} = 72.6$ μdef). Similar design calculations based on the colder equivalent temperatures obtained in Table 19(b) give thinner design thicknesses, corresponding to a small reduction of 3 and 6 mm for the standard and laboratory fatigue laws respectively.

The AASHTO fatigue law is far more permissive, given that the $\varepsilon_{t\ admis}$ (72.7 μdef for 20 cm of asphalt and $FC=0.2$) increases as the asphalt thickness decreases, allowing a total asphalt thickness as low as 10.5 cm ($\varepsilon_{t\ admis} = 124.9$ μdef). However, it is important to note that GB 20 asphalt would not be selected for such a thin pavement.

Calculations made with the equivalent temperature representative of EICM unbound layer moduli variations show a negligible (1-2 mm) increase in design thicknesses (cf. Table 20). The smallness of these differences can be explained by the compensatory effect of frost strengthening and thaw weakening in the damage assessment.

² The following rule is used for all SERUL design thickness calculations in this study: adjust ESG 10 thickness to no less than 4 cm, then reduce GB 20 if further reduction is needed.

The bottom part of Table 20 presents the results from the same analysis performed with the AASHTOWare PMED software. The differences between both software packages range from 9 to 14% in terms of design life and from 2 to 4 mm in terms of design thickness.

6.6. Additional verification of the structure at the SERUL site using the AASHTOWare PMED software

The French method does not take seasonal moisture and freeze/thaw variations into account for the subgrade and all other unbound layers; instead, they are given a constant modulus during the whole design period. In contrast, the AASHTOWare PMED software, with its climate model (EICM), allows variations in the modulus to be taken into account for all layers depending on their moisture content and temperature and the freeze/thaw cycle.

In the previous section, the EICM modulus predictions have been used to determine alternative θ_{eq} values, allowing integration of these features into the French method for bottom-up fatigue cracking.

Additional features of the AASHTOWare PMED software include predictions of top-down cracking, thermal cracking, rutting and roughness index (IRI). Calculations were made for these models, along with bottom-up fatigue cracking predictions, using the hourly climatic data and the AC modulus parameters from Table 10. For comparison purposes, the calculations were made in two ways regarding unbound materials, firstly with constant moduli for the whole year and secondly with the seasonal variations predicted by the EICM module. These modulus simulations are illustrated in Figure 16, (a) and (b) respectively, and the results are summarized in Table 21.

The bottom-up fatigue cracking predictions are similar for the two unbound material modeling conditions; as expected, fatigue design thicknesses (10.0 and 9.7 cm) are very similar to the previous results based on the concept of equivalent temperature (10.3 to 10.6 cm in Table 20 for the AASHTO fatigue law).

Top-down cracking results should not be interpreted because the very high value was unstable when applying minor changes in asphalt thickness. Also, this model will be replaced by a completely different one in the next version (2.6) of the software.

The predicted thermal cracking is very low and almost the same for the two conditions. A 27% increase in rutting, from 7.8 to 9.9 mm, is predicted when using variable unbound layer moduli. We can conclude from these results that spring thaw effects are more detrimental to rutting than winter frost strengthening is beneficial. When looking at the design thickness, the EICM unbound modulus variations cause rutting criteria to become more critical than fatigue, with a minimum thickness rising from 7.4 to 13.8 cm. This last, and highest, AASHTOWare PMED thickness is significantly lower than the 18 to 20 cm required by the French and laboratory fatigue laws.

7. Conclusions and future prospects

This study looked at the hypotheses used in bituminous pavement design using two mechanistic-empirical methods (French and US). Several differences and similarities have been enumerated and described.

The main focus was a comparison of the fatigue models for bituminous mixes as a function of temperature. Equivalencies have been found, as well as methods to import the layers moduli and fatigue model from a method to the other. The coefficients of the French fatigue law have been ported to the coefficients available in the AASHTOWare PMED. Conversely, an "aggregated AASHTO" pavement fatigue law was formulated to be compatible with the equivalent temperature θ_{eq} approach used by the Alizé-LCPC software. To achieve this, a second equivalent temperature θ_{eq2} needed to be determined, with respect to the aging and traffic loading frequency models included in the AASHTOWare PMED software. The equivalent temperature has been demonstrated to be an efficient parameter that includes the results of a detailed hourly analysis.

The results made it possible to assess the effect of climate on pavement performance at a site in France and a site in Québec.

For the A63 express highway section near Bordeaux in France, the criterion that leads to failure is the fatigue cracking of asphalt mixes. This remains true when the Seattle and Phoenix (United States) climates are applied. Structural fatigue damage increases with

temperature. The design results show that both the US and the French methods gave similar results and trends in terms of asphalt thickness. However, the US method appeared more conservative for the warmer climate of Phoenix. Also it was noted that the US fatigue law tends to become more permissive for thinner pavements, which would have a significant impact on the design of lower traffic roads and may increase the need or relevance of additional rutting and degradation models.

The calculations showed the importance of taking climate conditions into account, as well as the choice and calibration of degradation models.

In addition, the climate does not solely affect the temperature of the asphalt mix. The results for the site in Québec show that, if the effect of moisture and the freeze/thaw cycle in the layers of unbound materials is taken into account, more severe permanent deformation is predicted. For this site, the rutting criterion was found to be most unfavourable using the AASHTOWare PMED software.

Last, this study provides an insight into the impact of the climate on bituminous pavement design using the French and US mechanistic-empirical methods. The calibration of the calculation methods and an appropriate choice of parameters are essential if realistic results are to be achieved. Interesting features of the two design methods have been outlined. Both packages are likely to evolve further in the coming years. Additional efforts will also be made to calibrate mechanistic-empirical pavement design methods according to local climatic conditions.

Acknowledgements

The authors thank Météo France for providing climate data, Professor Guy Doré from Université Laval for his assistance and data about the structure of the SERUL site, and the Pays de Loire region in France for financing the *Région RI-ADAPTCLIM* project.

Conflict of interest

None

References

- A. Elshaeb, M., M. El-Badawy, S., A. Shawaly, E.-S., 2014. Development and Impact of the Egyptian Climatic Conditions on Flexible Pavement Performance. *Am. J. Civ. Eng. Archit.* 2, 115–121. <https://doi.org/10.12691/ajcea-2-3-4>
- AAPT, 2016. State of the Art and Practice in Fatigue Cracking Evaluation of Asphalt Concrete Pavements Version 1.0 An experimental and numerical synthesis from the mid-1990s to 2016.
- AASHTO, 2018. Enhancements to the mechanistic-empirical pavement design guide. Addendum number FY2018.4, Revised model/global calibration coefficients from recalibration. June 30, 2018. <https://me-design.com/MEDesign/Documents.html> Recalibration Addendum 4 MOP (docx) [7/10/2018].
- AASHTO, 2015. Mechanistic-empirical pavement design guide: a manual of practice., American Association of State Highway and Transportation Officials. ed.
- AASHTO, 2008. Mechanistic-empirical pavement design guide: A manual of practice. Washington, DC.
- AASHTO, 1993. Guide for Design of Pavement Structures. American Association of State Highway and Transportation Officials, Washington, D.C.
- Badiane, M., 2016. Effet des charges sur les chaussées en période de restriction des charges-volet terrain (Mémoire de maîtrise en génie civil). Université Laval, Québec Canada.
- Balay, J.M., Brosseaud, Y., BARA, B., Castaneda, E., 2012. Adaptation of the French pavement design to countries in South America, in: Congrès 8eme Jornadas International Des Asfalto. France, p. 14p.
- Bilodeau, J.P., Doré, G., Thiam, P.M., Perron Drolet, F., 2013. Long-term performance of flexible pavement structures in changing climate. Presented at the Annual Conference of the Transportation Association of Canada, Winnipeg, Manitoba.
- Bodin, D., Terrier, J.-P., Perroteau, C., Hornych, P., Marsac, P., 2010. Effect of temperature on fatigue performances of asphalt mixes. Presented at the 11th International Conference on Asphalt Pavements, At Nagoya, Japan.
- Burmister, D.M., 1945. The General Theory of Stresses and Displacements in Layered Soil Systems. II. *J. Appl. Phys.* 16, 126–127. <https://doi.org/10.1063/1.1707562>
- Canada, Government of, 2018. Environment and natural resources - Weather data - Historical climate data [WWW Document]. URL https://climate.weather.gc.ca/historical_data/search_historic_data_e.html (accessed 3.1.18).

- Carpenter, S.H., 2006. Fatigue performance of IDOT mixtures (Research Report No. FHWA-ICT-07-007). University of Illinois at Urbana-Champaign, Illinois Center for Transportation.
- Chailleux, E., 2007. User Manual of Visco-Analysis Software. LCPC.
- Copper, K.E., Pell, P.S., 1974. The effect of mix variables on the fatigue strength of bituminous materials.
- de Mello, L.G.R., de Farias, M.M., Kaloush, K.E., 2016. Effect of temperature on fatigue tests parameters for conventional and asphalt rubber mixes. *Road Mater. Pavement Des.* 1–14. <https://doi.org/10.1080/14680629.2016.1261728>
- Di Benedetto, H., De La Roche, C., Baaj, H., Pronk, A., Lundström, R., 2004. Fatigue of bituminous mixtures. *Mater. Struct.* 37, 202–216.
- Diakhaté, M., Millien, A., Petit, C., Phelipot-Mardelé, A., Pouteau, B., 2011. Experimental investigation of tack coat fatigue performance: Towards an improved lifetime assessment of pavement structure interfaces. *Constr. Build. Mater.* 25, 1123–1133. <https://doi.org/10.1016/j.conbuildmat.2010.06.064>
- Domec, V., 2005. Endommagement par fatigue des enrobés bitumineux en condition de trafic simulé et de température (Thèse de doctorat). Université de Bordeaux 1.
- Domec, V., Breyse, D., Roche, C. de L., Yotte, S., 2005. Caractérisation de la durée de vie en fatigue des enrobés bitumineux en conditions de « trafic simulé » et de température. *Rev. Eur. Génie Civ.* 9, 385–400. <https://doi.org/10.1080/17747120.2005.9692761>
- Doré, G., Bilodeau, J.-P., Thiam, P.M., Drolet, F.P., 2014. Impact des changements climatiques sur les chaussées des réseaux routiers québécois (Département de génie civil et de génie des eaux Université Laval).
- Doucet, F., 1999. Caractérisation de la rigidité et de la résistance à la fatigue des enrobés. Université de Sherbrooke.
- Dumont, A.G., Bressi, S., 2014. *Fahrbahn bemessung: derzeitiger Zustand und Entwicklung - (FR) Dimensionnement des chaussées: état actuel et évolution.* Str. Verk. 100.
- El-Basyouny, M., Witczak, M., 2005. Part 2: Flexible Pavements: Calibration of Alligator Fatigue Cracking Model for 2002 Design Guide. *Transp. Res. Rec. J. Transp. Res. Board* 1919, 76–86. <https://doi.org/10.3141/1919-09>
- Enríquez-de-Salamanca, Á., 2017. Environmental impacts of climate change adaptation of road pavements and mitigation options. *Int. J. Pavement Eng.* 1–6.
- Finn, F., Saraf, C., Kulkarni, R., Nair, K., Smith, W., Abdullah, A., 1977. The use of distress prediction subsystems for the design of pavement structures. Presented at

- the Volume I of proceedings of 4th International Conference on Structural Design of Asphalt Pavements, Ann Arbor, Michigan, August 22-26, 1977.
- Francken, L., Verstraeten, J., 1994. Interlaboratory Test Program – Part II, Repeted Loading Tests. Draft Rep. RILEM TC 152 PBM – Perform. Bitum. Mix.
- Gudipudi, P.P., Underwood, B.S., Zalghout, A., 2017. Impact of climate change on pavement structural performance in the United States. *Transp. Res. Part Transp. Environ.* 57, 172–184. <https://doi.org/10.1016/j.trd.2017.09.022>
- Hasan, M.A., Tarefder, R.A., 2017. Development of temperature zone map for mechanistic empirical (ME) pavement design. *Int. J. Pavement Res. Technol.*
- Hasan, M.R.M., Hiller, J.E., You, Z., 2016. Effects of mean annual temperature and mean annual precipitation on the performance of flexible pavement using ME design. *Int. J. Pavement Eng.* 17, 647–658. <https://doi.org/10.1080/10298436.2015.1019504>
- Hornych, P., Balay, J.M., Mauduit, C., Bodin, D., 2013. Evaluation of the concept of equivalent temperature for pavement design, in: *Proceedings of the 9th International Conference on the Bearing Capacity of Roads, Railways and Airfields (BCRRA 2013)*. At Trondheim, Norway, pp. 319–329.
- Islam, M.R., Tarefder, R.A., 2015. Quantifying Traffic- and Temperature-Induced Fatigue Damages of Asphalt Pavement. *Transp. Infrastruct. Geotechnol.* 2, 18–33. <https://doi.org/10.1007/s40515-014-0014-3>
- LCPC-SETRA, 1998. *Catalogue des structures types de chaussées neuves*. Ministère de l'Équipement, des Transports et du Logement.
- LCPC-SETRA, 1994. *Conception et dimensionnement des structures de chaussée*. Ministère de l'Équipement des Transports et du Tourisme, Paris.
- Lundstrom, R., Di Benedetto, H., Isacsson, U., 2004. Influence of Asphalt Mixture Stiffness on Fatigue Failure. *J. Mater. Civ. Eng.* 16, 516–525. [https://doi.org/10.1061/\(ASCE\)0899-1561\(2004\)16:6\(516\)](https://doi.org/10.1061/(ASCE)0899-1561(2004)16:6(516))
- Marsac, P., 2018. Evolutions des performances des matériaux vieilliss. Presented at the Restitution des résultats de l'ORSI “DEDIR” du Dimensionnement à l'Entretien Durable des Infrastructures Routières, IFSTTAR, Nantes.
- Marsac, P., El-Bedoui, S., Larriere, A., 2010. Influence de la température sur la caractérisation en fatigue d'un enrobé bitumineux (Opération de recherche No. 11P063).
- Meyer, M., Flood, M., Keller, J., Lennon, J., McVoy, G., Dorney, C., Leonard, K., Hyman, R., Smith, J., National Cooperative Highway Research Program, Transportation Research Board, National Academies of Sciences, Engineering, and Medicine, 2014. *Strategic Issues Facing Transportation, Volume 2: Climate Change, Extreme Weather Events, and the Highway System: Practitioner's Guide and Research*

- Report. Transportation Research Board, Washington, D.C.
<https://doi.org/10.17226/22473>
- Miner, M.A., 1945. Cumulative Damage in Fatigue. *J. Appl. Mech.* 159–164.
- Mirza, M.W., Witczak, M.W., 1995. Development of a Global Aging System for Short and Long Term Aging of Asphalt Cements. *J. Assoc. Asph. Paving Technol.* 64, 393–430.
- Monismith, C.L., 2004. Evolution of Long-Lasting Asphalt Pavement Design Methodology: A Perspective, in: *Distinguished Lecture International Society for Asphalt Pavements*. Presented at the International Symposium on Design and Construction of Long Lasting Asphalt Pavements, Alabama, USA, p. 77.
- Moutier, F., 1991. Etude statistique de l'effet de la composition des enrobés bitumineux sur leur comportement en fatigue et leur module complexe (Bulletin de liaison des laboratoires des Ponts et Chaussées No. n°172).
- Nasimifar, S.M., Pouranian, M.R., Azadi, M., 2011. The Effect of Climatic Conditions of Various Regions of Iran on Pavement Fatigue Cracking. *ACEEE Int J Transp. Urban Dev.* 01. <https://doi.org/01.IJTUD.01.01.27>
- NCHRP, 2004. Guide for mechanistic-empirical design of new and rehabilitated pavement structures, final document, Appendix II-1: Calibration of fatigue cracking models for flexible pavements (National Research Council No. NCHRP Project 1-37A,). Washington, DC.
- Pereira, P., Pais, J., 2017. Main flexible pavement and mix design methods in Europe and challenges for the development of an European method. *J. Traffic Transp. Eng. Engl. Ed., Special Issue on Maintenance and Rehabilitation of Pavements* 4, 316–346. <https://doi.org/10.1016/j.jtte.2017.06.001>
- Perraton, D., Baaj, H., Carter, A., 2010. Comparison of Some Pavement Design Methods from a Fatigue Point of View: Effect of Fatigue Properties of Asphalt Materials. *Road Mater. Pavement Des.* 11, 833–861. <https://doi.org/10.1080/14680629.2010.9690309>
- Perraton, D., Di Benedetto, H., Carter, A., Proteau, M., 2019. Link between different bottom-up fatigue's law coefficients of mechanical-empirical pavement design software. *Constr. Build. Mater.* 216, 552–563. <https://doi.org/10.1016/j.conbuildmat.2019.04.256>
- Roy, M., St-Laurent, D., Bergeron G., 1997. Seasonal variations of pavements: a FWD study. XIIIth World meeting of the International Road Federation, Toronto, Canada.

- Rychen, P., 2013. Impact du changement climatique sur les infrastructures routières: analyse de risque et mesures d'adaptation (Docteur Ès Sciences). École Polytechnique Fédérale De Lausanne, Suisse.
- Saha, J., Nassiri, S., Bayat, A., Soleymani, H., 2014. Evaluation of the effects of Canadian climate conditions on the MEPDG predictions for flexible pavement performance. *Int. J. Pavement Eng.* 15, 392–401.
- Silva, H.M., Oliveira, J.R., Picado-Santos, L.G., 2008. Influence of temperature on the fatigue life of flexible pavements. *Proc. 3RD Eur. Pavement Asset Management Conf. EPAM3 7-9 JULY 2008 Coimbra, Portugal.*
- Such, C., 1983. Analyse du comportement visqueux des bitumes. *Bulletin de liaison des laboratoires des ponts et chaussées, France.*
- Tayebali, A.A., Deacon, J.A., Coplantz, J.S., Finn, F.N., Monismith, C.L., 1994. Fatigue Response of Asphalt-Aggregate Mixes. Part II- Extended Test Program. Asphalt Research Program. Institute of Transportation Studies, University of California, Berkeley, Strategie Highway Research Program , National Research Council. ed, Rapport SHRP-A-404. Washington, D.C.
- Touhara, R., 2012. Étude de la résistance en fatigue des matériaux bitumineux (Maitrise en Génie de la construction). École de technologie supérieure.
- Wei, L., Kayser, S., Wellner, F., 2013. Impact of Surface Temperature on Fatigue Damage in Asphalt Pavement. *J. Highw. Transp. Res. Dev. Engl. Ed.* 7, 1–6.
- Williams, M.L., Landel, R.F., Ferry, J.D., 1955. The Temperature Dependence of Relaxation Mechanisms in Amorphous Polymers and Other Glass-forming Liquids. *J. Am. Chem. Soc.* 77, 3701–3707. <https://doi.org/10.1021/ja01619a008>
- Wistuba, M.P., Walther, A., 2013. Consideration of climate change in the mechanistic pavement design. *Road Mater. Pavement Des.* 14, 227–241. DOI: 10.1080/14680629.2013.774759
- Yang X., You Z., Hiller J., Watkins D., 2015. Sensitivity of flexible pavement design to Michigan's climatic inputs using pavement ME design. *International Journal of Pavement Engineering*, DOI: 10.1080/10298436.2015.1105373
- Yang X., You Z., Hiller J., Watkins D., 2016. Updating and augmenting weather data for pavement mechanistic-empirical design using ASOS/AWOS database in Michigan. *International Journal of Pavement Engineering*, DOI: 10.1080/10298436.2016.1234278
- Yang X., You Z., Hiller J., Watkins D., 2017. Correlation Analysis between Temperature Indices and Flexible Pavement Distress Predictions Using Mechanistic-Empirical Design. *J. Cold Reg. Eng.* 31, 04017009. DOI: 10.1061/(ASCE)CR.1943-5495.0000135

Yu, J., Tsai, B.-W., Zhang X., Monismith, C., 2012. Development of asphalt pavement fatigue cracking prediction model based on loading mode transfer function. *Road Mater. Pavement Des.* 13, 501–517. DOI: 10.1080/14680629.2012.695240

Table 1. Value of coefficient k_c

Material	Gravel/Bitumen mix (GB)	Bituminous concrete	High modulus asphalt (EME)
k_c	1.3	1.1	1

Table 2. Value of coefficient k_s

Class of working platform	PF1	PF2	PF3	PF4
Modulus (MPa)	20 to 50	50 to 120	120 to 200	Over 200
k_s	1/1.2	1/1.1	1	1

Table 3 . Differences between software packages

	<p>Alizé-LCPC v 1.5</p> 	<p>AASHTOWare Pavement ME Design v 2.5</p> 
Climate	<ul style="list-style-type: none"> - Calculations using an equivalent temperature (Miner's law) - Constant modulus for unbound material layers 	<ul style="list-style-type: none"> - Calculations for each hourly temperatures (Miner's law applied on monthly temperature quintiles) - Global aging system - Temperature/frequency/aging gradients (EICM, subdivision of layers) - Variable moduli for unbound material layers (EICM, moisture and freeze/thaw effects)
Traffic	<ul style="list-style-type: none"> - Equivalent single axle load (ESAL) 	<ul style="list-style-type: none"> - Calculated for each axle (Miner's law)
Fatigue	<ul style="list-style-type: none"> - Concept of statistical risk (r) - Correction factor for soil - Lateral wander included in calibration coefficient k_c - Failure at 50% cracking 	<ul style="list-style-type: none"> - Concept of statistical reliability ($R = 1 - r$) - Correction factors for thickness of bituminous mix - Lateral wander dealt with separately from the fatigue law (Miner's law, statistical grid pattern) - Empirical transfer function to convert damage ratio in terms of area of alligator fatigue cracking
Rutting	<ul style="list-style-type: none"> - Subgrade: $\varepsilon_{z, ad} = 0,012(NE)^{-0,222}$ 	<ul style="list-style-type: none"> - Each layer $\sum f(\varepsilon_z, h, T, W\dots)$
Other		<ul style="list-style-type: none"> - Top-down fatigue cracking - Transverse thermal cracking - Smoothness (IRI)

Table 4. Reference axles

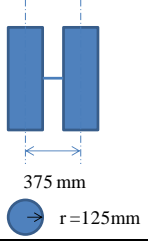
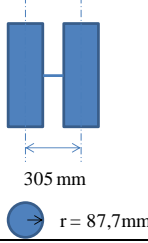
	ESAL ₁₃₀ A63, Bordeaux (130 kN)	ESAL ₈₀ SERUL, Québec (80 kN)
Standard dual tires		
Tire pressure (kPa)	662	827.4

Table 5. Calibrated parameters for bitumen

Bitumen	Huet-Such model									A-VTS model	
	G_{∞} (MPa)	k	h	δ	τ_0	β	A_0	A_1	A_2	A	VTS
35/50 (A63)	1985.1	0.29	0.67	4.48	0.28	22.02	-1.115	-0.399	0.002	9.8196	-3.2519
PG 58-34 (SERUL)	1995.3	0.33	0.70	8.09	0.00	599.23	-5.833	-0.328	0.002	8.5728	-2.8031

Table 6. Traffic frequency estimated at layer mid-depth (NCHRP, 2004)

Operating speed (km/h)	Estimated frequency at layer mid-depth (Hz)		
	Representative HMA layer (100 – 300 mm)	Thin HMA layer wearing surface (25 – 75 mm)	Thick HMA layers binder/base (75 – 300 mm)
100	15-40	45-95	10-25
70	10-30	35-70	15-20
25	5-10	10-25	5-10
1	0.1-0.5	0.5-1.0	0.1-0.25

Table 7. Measurement of the aging effect (two-point bending tests) (Marsac, 2018)

Type of bituminous mix	Parameter	1990	2014	Δ
GB	Modulus at 10 °C and 25 Hz (MPa)	15017	20367	+36%
	Modulus at 15 °C and 10 Hz (MPa)	10292	16868	+64%
	ε_6 ($\mu\text{m/m}$)	88	111	+26%
	-1/b	4.3	8.3	+93%
EME	Modulus at 10 °C and 25 Hz (MPa)	16553	20694	+25%
	Modulus at 15 °C and 10 Hz (MPa)	12406	17337	+40%
	ε_6 ($\mu\text{m/m}$)	140	141	+0.7%
	-1/b	5.3	7.4	+40%

Table 8. Summary of hourly temperatures, A63 Bordeaux (August 1, 2003 to August 1, 2013)

(°C)	Air	Surface	10 cm	20 cm	30 cm	50 cm	70 cm	1 m
Min	-8.1	-11.9	-8.0	-4.9	-2.7	0.2	1.9	4.9
Mean	13.8	16.1	16.0	16.0	16.0	16.0	16.0	16.0
Max	38.7	51.6	42.5	37.3	34.3	31.3	29.8	27.5

Table 9. Parameters of bituminous mixes for design using the Alizé-LCPC software

Site	Bituminous mix	E(MPa) at 15 °C and 10Hz	ν	ϵ_6 (10 °C, 25Hz)	-1/b	n	k_c	E(MPa) at 10Hz					
								-10 °C	0 °C	10 °C	20 °C	30 °C	40 °C
A63	BBSG 3	7000	0.35	100	5	0.5	1.1	16000	13500	9310	4690	1800	1000
	GB 3	9000	0.35	90	5	0.5	1.3	22800	18300	11880	6120	2700	1000
SERUL	ESG 10	6000	0.35	---	---	---	1	21170	15050	8670	3950	1500	530
	GB 20	7400	0.35	186	4.23	0.3806	1	19830	15250	9950	5200	2130	700

Table 10. Parameters for dynamic moduli according to AASHTOWare PMED (cf. (Eq.16))

	A63, Bordeaux, France		SERUL, Québec, Canada	
	BBSG 3	GB 3	ESG 10	GB 20
δ	4.1155	-5.5974	2.6164	0.7201
α	2.3333	12.3067	4.0359	5.8505
β	-0.35813	-2.38804	-0.77145	-1.54109
γ	0.57731	0.29534	0.39942	0.36455
c	1.23985	1.48977	1.65163	1.79033
SSE	0.02796	0.00138	0.01371	0.02711
Se/Sy	0.08232	0.01711	0.02075	0.02882

Table 11. Calculation of equivalent temperature θ_{eq} at different time increments – A63 Bordeaux

Fatigue law	Year	Hourly (8760 hours)	Daily (365 days)	Weekly (52 weeks)	Monthly (12 months)
GB 3 (LCPC-SETRA, 1994)	2004	19.1	18.6	18.4	18.2
	2006	19.8	19.5	19.3	19.2
	2008	18.5	18.0	17.8	17.6
GB 3 LCPC Experimental (Bodin et al., 2010)	2004	19.6	19.3	19.1	19.8
	2006	20.8	20.4	20.1	20.2
	2008	19.1	18.7	18.6	18.8
(AASHTO, 2018)	2004	18.1	17.7	17.5	17.4
	2006	18.7	18.4	18.3	18.2
	2008	17.6	17.2	17.0	16.9
SHRP (Tayebali et al. 1994)	2004	18.2	17.9	17.8	18.8
	2006	18.5	18.3	18.2	18.9
	2008	17.8	17.5	17.5	17.9
ESG 14 conv (Doucet, 1999)	2004	16.0	15.4	15.4	17.1
	2006	16.7	16.2	16.1	17.1
	2008	15.9	15.4	15.4	16.2

Table 12. Equivalent temperature for various EICM climate simulations (A63, 240 months)

a) θ_{eq} based on EICM predicted AC temperatures (E recalculated for 10 Hz, no aging)

Fatigue law	AASHTOWare temperatures set	Seattle (MAAT = 10 °C)	Bordeaux (MAAT = 13.8 °C)	Phoenix (MAAT = 24 °C)
LCPC-SETRA	Mid-quintile	15.0	19.6	29.1
	All quintiles	16.5	21.1	29.1

b) θ_{eq2} based on EICM predicted AC moduli (variable frequency and aging)

Fatigue law	AASHTOWare moduli set	Seattle (MAAT = 10 °C)	Bordeaux (MAAT = 13.8 °C)	Phoenix (MAAT = 24 °C)
AASHTO aggregated	Mid-quintile	9.3	15.6	26.4
	All quintiles	11.4	17.1	27.3

Table 13. Simulations for various climates (A63, LCPC-SETRA fatigue law, both software packages)

Inputs	θ_{eq} (°C)	5	10	15 (Seattle)	19 (Bordeaux)	20	21	25	29 (Phoenix)	30	35	40
	Layer moduli (MPa)		11405 15090 120	9310 11880 120	7000 9000 120	5152 6696 120	4690 6120 120	4401 5778 120	3245 4410 120	2089 3042 120	1800 2700 120	1400 1850 120
Alizé	ϵ_t calc (μ def) *	32.8	39.6	49.5	62.4	66.9	69.9	86.0	113.5	123.7	157.7	224.7
	ϵ_t ad (μ def)	39.7	44.8	51.5	59.7	62.4	64.2	73.5	88.5	94.0	113.5	154.4
	Lifespan (years) *	41.7	32.3	23.4	16.6	15.0	14.1	10.3	6.8	6.0	4.7	3.8
	Min. thickness of GB 3 (cm) (20 years design)	22.2 -3.8	23.5 -2.5	25.2 -0.8	27.0 +1.0	27.6 +1.6	27.9 +1.9	29.6 +3.6	31.9 +5.9	32.6 +6.6	34.3 +8.3	36.0 +10.0
AASHTOWare	% fatigue cracking *	3.4	6.3	27.0	75.6	89.7	97.9	100	100	100	100	100
	Lifespan (years) *	41.6	32.4	23.6	16.8	15.2	14.2	10.4	6.9	6.1	4.8	3.8
	Min. thickness of GB 3 (cm) (20 years design)	22.3	23.6	25.2	27.0	27.5	27.9	29.5	31.7	32.4	34.0	35.6

*Note: ϵ_t and lifespan calculated for 8 cm BBSG and 26 cm GB 3.

Table 14. Fatigue model coefficients for the AASHTOWare PMED software

Context	Bituminous mix	Fatigue model	C·C _H	$\beta_{f1}k_{f1}$	$\beta_{f2}k_{f2}$	$\beta_{f3}k_{f3}$
A63 (see Figure 7a)	GB 3 V _b = 10.79% V _a = 9.0%	(AASHTO, 2018)	49.8 (0.199·250*)	$5.014 \left(\frac{h_{ac}}{2.54}\right)^{-3.416} \cdot 3.75$ [0.077 for h _{ac} < 12.7 cm, 0.00387 for h _{ac} ≥ 30.48 cm]	3.9606	1.2848
		(LCPC-SETRA, 1994)		$-0.01066 \left(\frac{h_{ac}}{2.54}\right)^2$ $+ 0.6524 \left(\frac{h_{ac}}{2.54}\right) - 1.1765$ [5.12 for h _{ac} ≥ 30.48 cm]	5	2.5
SERUL (see Figure 7b)	GB 20 V _b = 10.2% V _a = 5.8%	(AASHTO, 2018)	139.3 (0.557·250*)	$5.014 \left(\frac{h_{ac}}{2.54}\right)^{-3.416} \cdot 3.75$ [0.077 for h _{ac} < 12.7 cm, 0.0163 for h _{ac} = 20 cm, 0.00387 for h _{ac} ≥ 30.48 cm]	3.9606	1.2848
		(LCPC-SETRA, 1994)		$-0.1151 \left(\frac{h_{ac}}{2.54}\right)^2 +$ $4.862 \left(\frac{h_{ac}}{2.54}\right) - 6.7667$ [24.4 for h _{ac} = 20 cm, 35.0 for h _{ac} ≥ 30.48 cm]	5	2.5
		(Doucet , 1999)		$-0.00034194 \left(\frac{h_{ac}}{2.54}\right)^2$ $+ 0.014448 \left(\frac{h_{ac}}{2.54}\right)$ $- 0.020109$ [0.0725 for h _{ac} = 20 cm, 0.104 for h _{ac} ≥ 30.48 cm]	4.23	1.61

Note: *C_H = 250 for h_{ac} > 12.5 cm (Eq.9)

Table 15. Results of simulations for various climates – A63 (AASHTOWare PMED)

a) Degradations after 20 years (with 26 cm GB 3 and 99% reliability)

Degradation mode	Seattle (MAAT = 10 °C)	Bordeaux (MAAT = 13.8 °C)	Phoenix (MAAT = 24 °C)
Bottom-up fatigue cracking (%) AASHTO 2018 fatigue law			
• Hourly temperatures	31.0	100	100
• E fixed at equivalent temperature θ_{eq2}	28.3	100	100
Top-down cracking			
• Version 2.5.5 (m/km)	154	255	711
• Version 2.6.0 beta (%)	9.1	8.6	19.7
Thermal cracking (m/km)	74	74	354
Rutting, bituminous mix (mm)	2.0	3.1	9.0
Rutting, total (mm)	5.4	6.6	12.9
IRI (m/km)	2.6	3.1	3.5

b) Lifespan (in years)

Degradation mode (threshold)	Seattle	Bordeaux	Phoenix
Bottom-up fatigue cracking (%) AASHTO 2018 fatigue law			
• Hourly temperatures	22.9	13.8	3.8
• E fixed at equivalent temperature θ_{eq2}	23.4	13.7	4.1
Top-down cracking			
• Version 2.5.5 (380 m/km)	> 60	36.8	5.6
• Version 2.6.0 beta (25%)	39.2	40.2	27.1
Thermal cracking (200 m/km)	> 60	> 60	9.6
Rutting, total (20 mm)	> 60	> 60	> 60
IRI (3 m/km)	25	20	8.8

c) Minimum thickness of GB 3 layer for 20 years (cm) (fatigue criterion only)

AASHTO 2018 fatigue law	Seattle	Bordeaux	Phoenix
Hourly temperatures	25.0	28.6	38.0
E fixed at equivalent temperature θ_{eq2}	25.1	28.5	37.0

Table 16. Results with aggregated AASHTO fatigue law and Alizé-LCPC software (A63)

Inputs	θ_{eq2} (°C)	11.4 (Seattle)	17.1 (Bordeaux)	27.3 (Phoenix)
	Layer moduli (MPa)	8663	6044	2577
		11074	7808	3620
Results		120	120	120
	ε_t calc (μ def) *	41.9	55.3	99.8
	ε_t ad (μ def)	43.9	49.2	63.1
	Lifespan (years) *	23.2	13.6	4.0
	Min. thickness of GB 3 (cm) (20 years design)	25.1	28.6	37.3

*Note: ε_t and lifespan calculated for 8 cm BBSG and 26 cm GB 3.

Table 17. Summary of results for A63 (fatigue criterion only)

a) Predicted lifespans with 26 cm of GB 3 (years)

Software	Fatigue law	Seattle (10°/15°/11.4 °C)*	Bordeaux (13.8°/19°/17.1 °C)*	Phoenix (24°/29°/27.3 °C)*	Other climates
Alizé	LCPC- SETRA	23.4	16.6	6.8	See Table 13
	AASHTO	23.2	13.6	4.0	N/A
AASHTOWare	AASHTO**	[22.9 / 23.4]	[13.8 / 13.7]	[3.8 / 4.1]	N/A
	LCPC- SETRA	23.6	16.8	6.9	See Table 13

* (MAAT/ θ_{eq} / θ_{eq2}) **Based on [hourly temperatures / constant equivalent temperature θ_{eq2}]

b) Minimum design thickness of GB 3 layer for 20 years lifespan (cm)

Software	Fatigue law	Seattle (10°/15°/11.4 °C)*	Bordeaux (13.8°/19°/17.1 °C)*	Phoenix (24°/29°/27.3 °C)*	Other climates
Alizé	LCPC- SETRA	25.2	27.0	31.9	See Table 13
	AASHTO	25.1	28.6	37.3	N/A
AASHTOWare	AASHTO**	[25.0 / 25.1]	[28.6 / 28.5]	[38.0 / 37.0]	N/A
	LCPC- SETRA	25.2	27.0	31.7	See Table 13

* (MAAT/ θ_{eq} / θ_{eq2}) **Based on [hourly temperatures / constant equivalent temperature θ_{eq2}]

Table 18. Summary of daily temperatures, SERUL site (November 24, 2010 to June 27, 2017)

(°C)	Air	5 cm	10 cm	20 cm	30 cm	40 cm	60 cm	90 cm	110 cm	220 cm	300 cm
Min	-30.8	-24.1	-22.6	-20.7	-18.8	-16.9	-14.4	-11.3	-9.7	-2.3	0.0
Mean	1.8	6.3	6.2	6.2	6.0	5.9	5.8	5.7	5.7	5.9	5.7
Max	23.0	31.7	28.4	28.0	26.7	24.9	23.6	21.3	20.0	14.4	12.3

Table 19. Results of the equivalent temperature calculation (°C) - SERUL

a) Based on AC temperature measurements (Nov 2010 to June 2017)

Fatigue law (GB20)	Daily	Weekly	Monthly
LCPC-SETRA (1994)	11.3	11.1	11.1
Labo (Doucet, 1999)	12.5	12.4	12.3

b) Based on AC temperature/moduli predicted by AASHTOWare PMED

Period	Unbound layers	θ_{eq}		θ_{eq2}
		LCPC-SETRA	Labo	AASHTO
Mid-quintile	Constant Mr (no freeze/thaw)	8.5	9.4	2.6
All-quintiles		9.6	10.6	4.7
Mid-quintile	EICM variation (freeze/thaw)	8.7	9.7	2.5
All-quintiles		10.2	11.1	5.3

Table 20. Bottom-up fatigue analysis based on θ_{eq} and θ_{eq2} – SERUL (both software packages)

Inputs	AC temperatures	Measured		Generated by EICM from atmospheric hourly climate data					
	Unbound layers	Constant Mr (no freeze/thaw, cf. Figure 16a)				EICM variation (freeze/thaw, cf. Figure 16b)			
	Fatigue law	LCPC- SETRA	Labo	LCPC- SETRA	Labo	AASHTO	LCPC- SETRA	Labo	AASHTO
	θ_{eq} (°C)*	11.3	12.5	9.6	10.6	4.7 (θ_{eq2})	10.2	11.1	5.3 (θ_{eq2})
	Equivalent layers moduli (MPa)	7930 9270 250 109 54	7275 8660 250 109 54	8900 10160 250 109 54	8325 9635 250 109 54	11955 12775 250 109 54	8555 9845 250 109 54	8040 9375 250 109 54	11565 12455 250 109 54
Alizé	ϵ_t calc (μ def) *	71.6	75.3	66.9	69.6	56.1	68.5	71.0	57.2
	ϵ_t ad (μ def)	80.0	72.6	76.4	69.7	72.7–124.9**	77.7	70.44	73.3–125.4**
	Lifespan (years) *	34.9	17.1	39.0	19.6	56.0	37.5	19.3	53.5
	Min. total AC (cm) (20 years design)	18.4	20.6	18.1	20.0	10.5	18.2	20.2	10.6
AASHTOWare	% fatigue cracking	2.7	21.8	2.1	15.8	1.3	2.3	17.3	1.4
	Lifespan (years) *	39.8	19.1	44.3	22.4	61.0	42.7	21.5	58.3
	Min. total AC (cm) (20 years design)	18.1	20.2	17.8	19.7	10.3	17.9	19.8	10.4

Notes: * θ_{eq} , ϵ_t calc and lifespan determined for 20 cm total AC thickness

**AASHTO variation of ϵ_t ad for AC thickness from 20 cm to the 20 years design thickness

Table 21. Effect of variations in the modulus of unbound layers – SERUL (AASHTOWare PMED)

Degradation mode	Hypothesis on modulus of unbound layers (hourly climate data)	
	Constant (no freeze/thaw)	EICM Variation (freeze/thaw)
Bottom-up fatigue cracking (%) (AASHTO 2018 fatigue law)	1.7	1.7
Top-down cracking <ul style="list-style-type: none"> • Version 2.5.5 (m/km) • Version 2.6.0 beta (%) 	50 11.3	(1370)* 11.3
Thermal cracking (m/km)	27	
Rutting, bituminous mix (mm)	2.7	2.6
Rutting, total (mm)	7.8	9.9
IRI (m/km)	2.5	2.6
Minimum total AC for 20 years lifespan (cm) <ul style="list-style-type: none"> • 20% bottom-up fatigue cracking limit • 12 mm rutting limit 	10.0 7.4	9.7 13.8

* Unstable oscillations: 2348 to 76 m/km when varying total AC thickness from 195 to 203 mm.

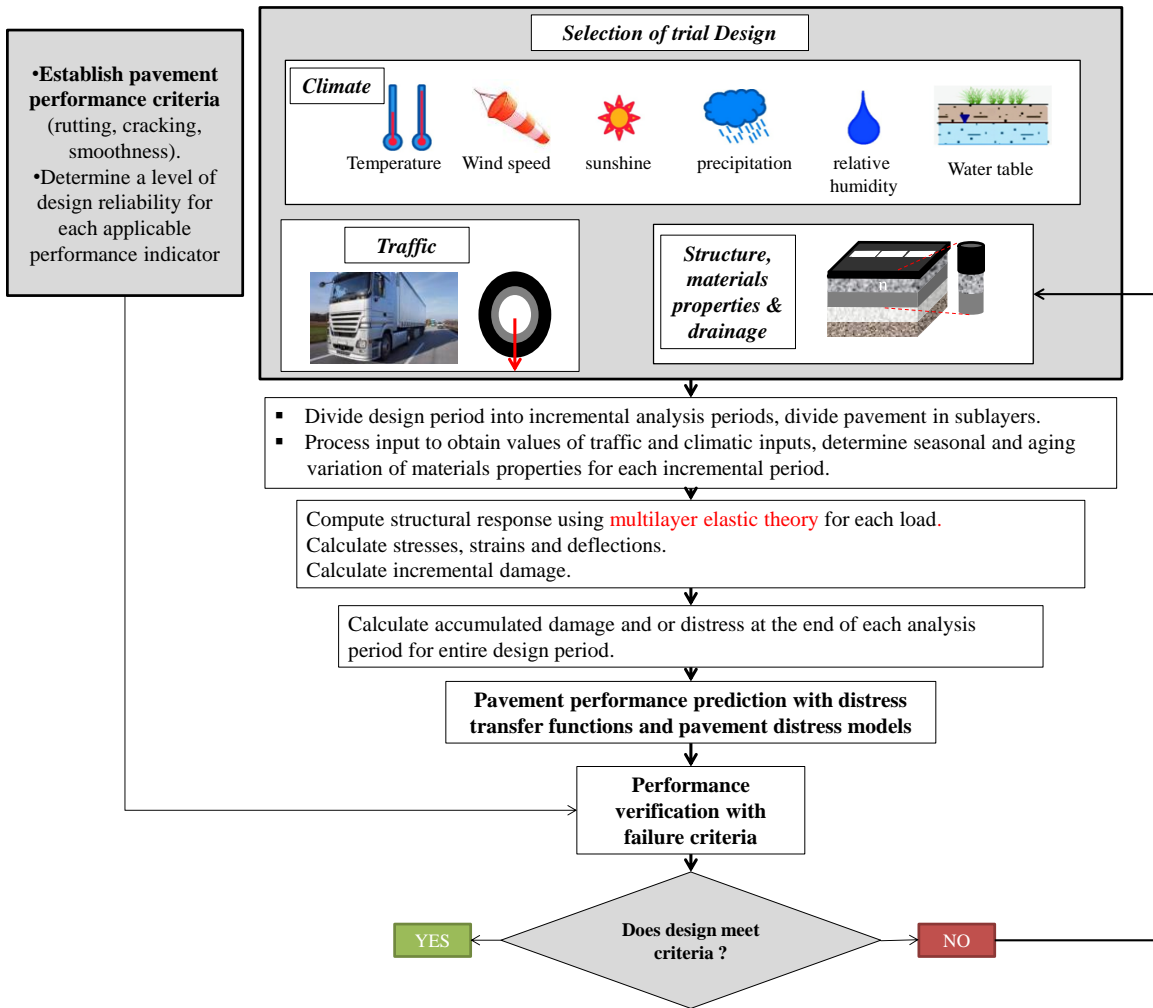


Figure 1. Mechanistic-empirical design process (AASHTO, 2015)

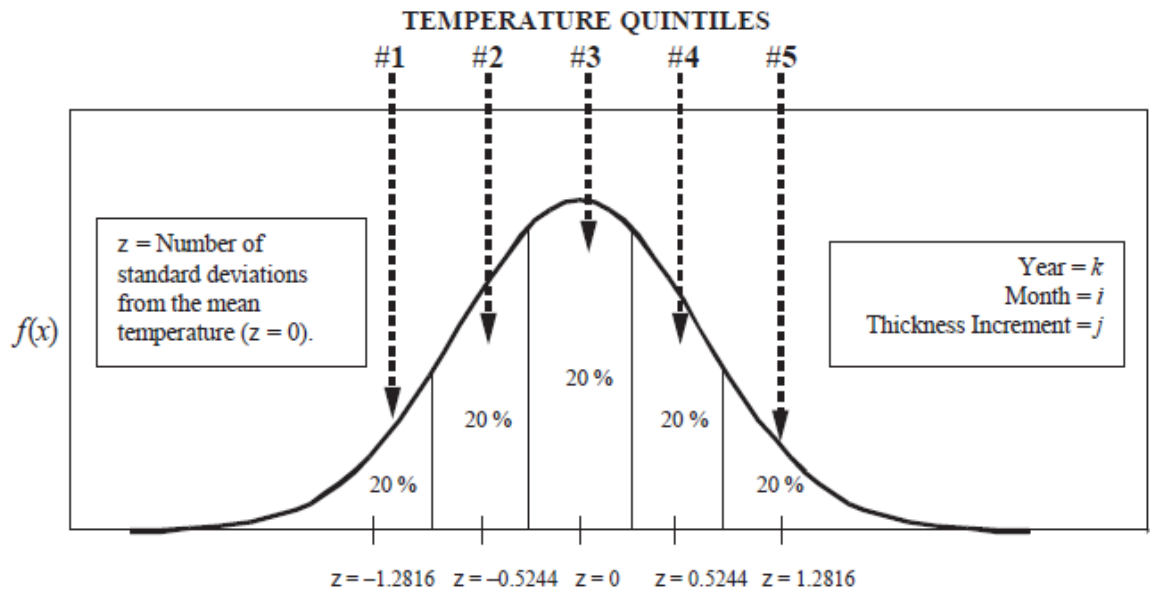
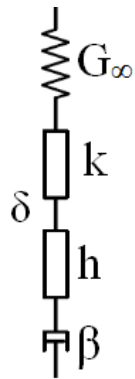


Figure 2. Subdivision of a month into temperature quintiles (AASHTO, 2015)



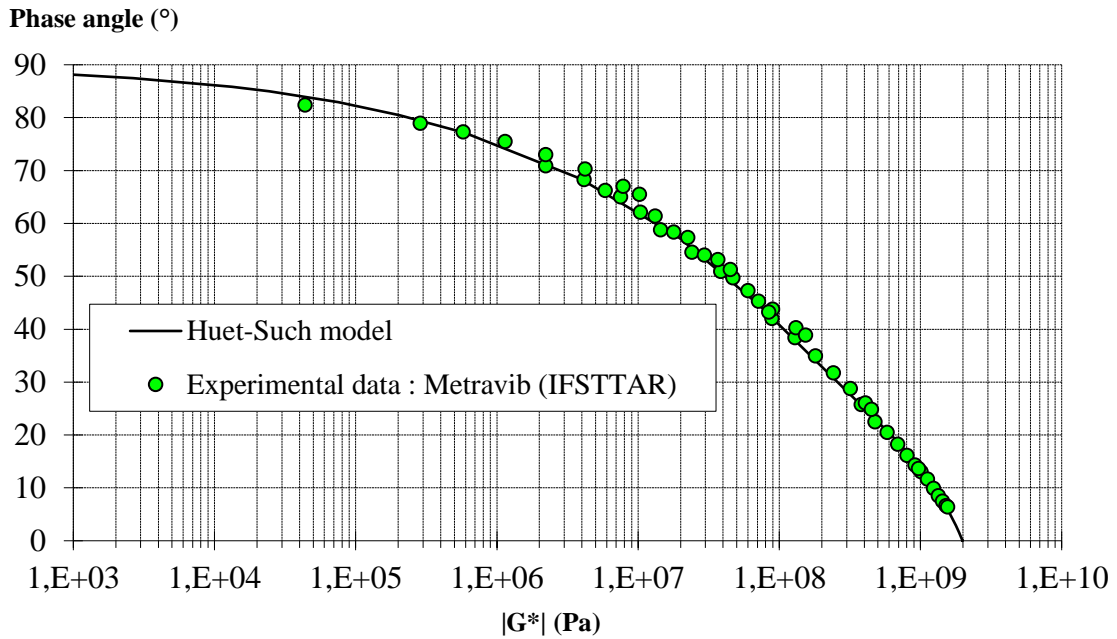
(a)

$$G^*(i\omega\tau) = \frac{G_\infty}{1 + \delta(i\omega\tau)^{-k} + (i\omega\tau)^{-h} + (i\omega\beta\tau)^{-1}}$$

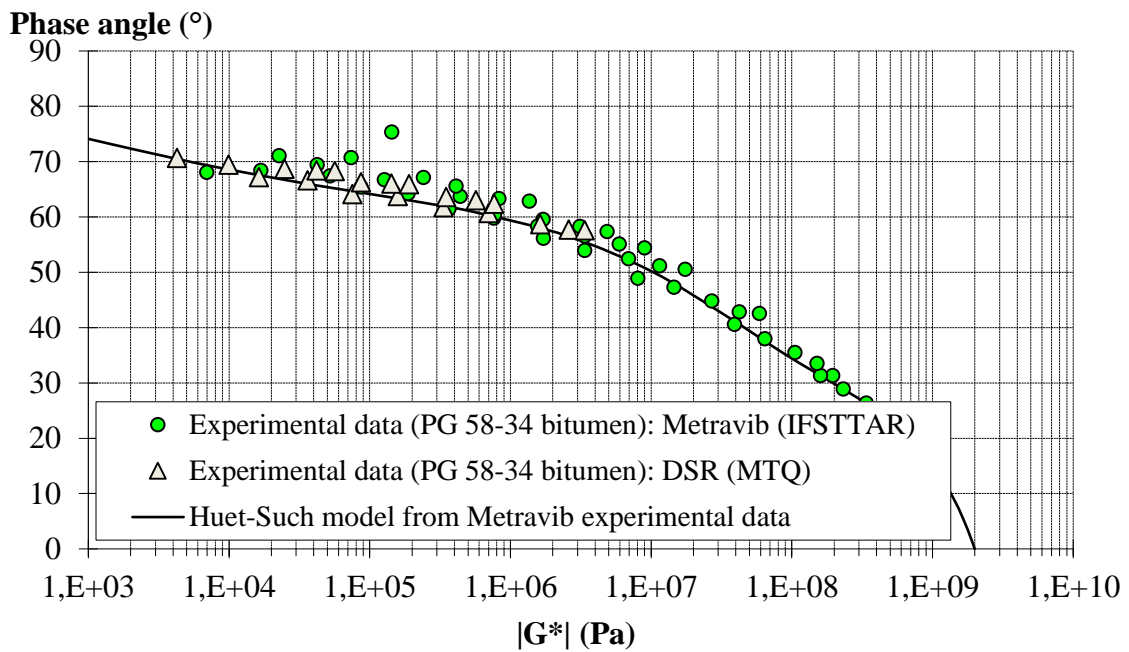
$$\tau(T) = e^{A_0 + A_1 T + A_2 T^2}$$

(b)

Figure 3. Huet-Such model, (a) Representation (b) Expressions



(a) 35/50 bitumen (A63 Bordeaux)



(b) 58-34 bitumen (SERUL)

Figure 4. Complex shear modulus master curve of binders in Black space

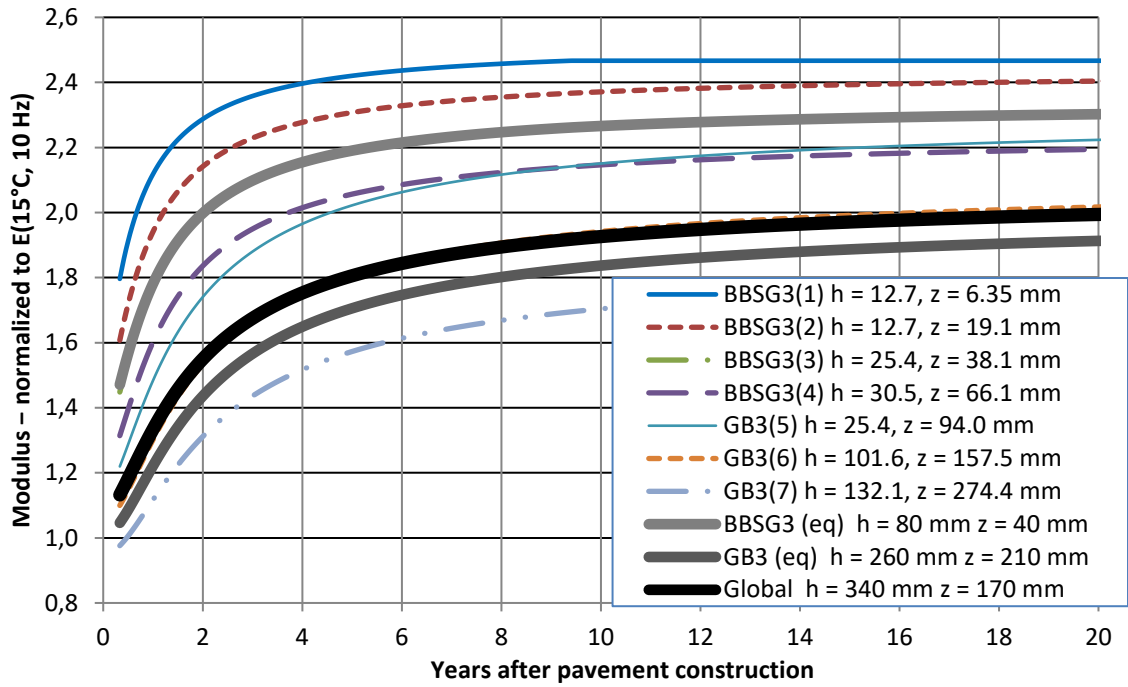


Figure 5. Aging simulation at a constant temperature of 15 °C (AASHTOWare PMED)

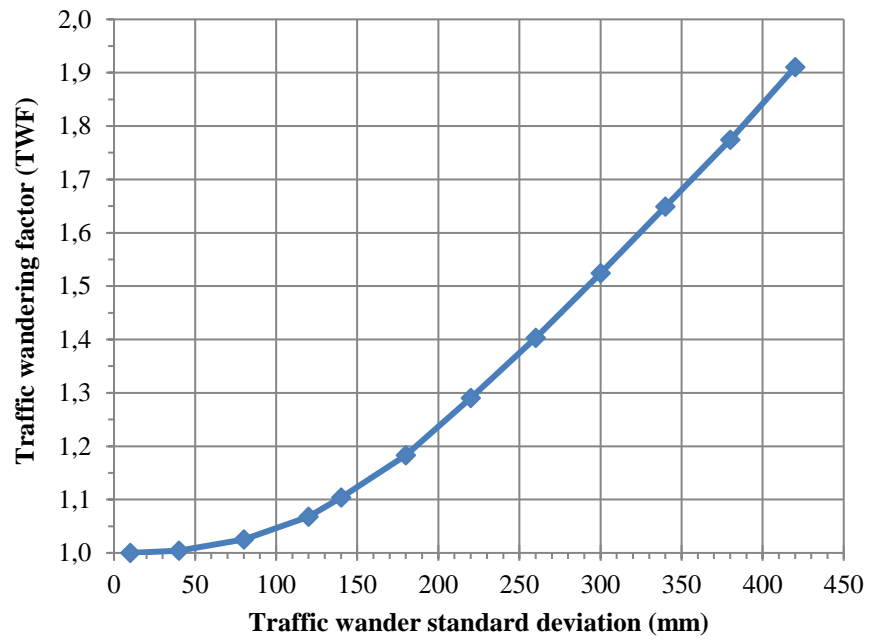
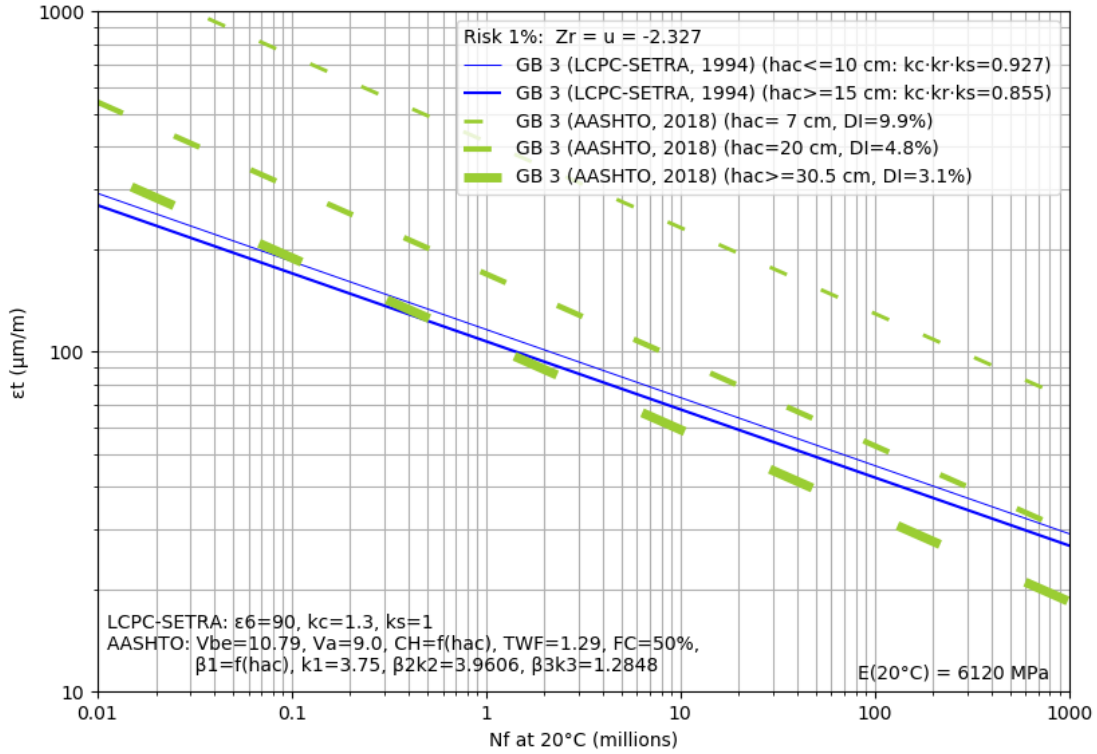
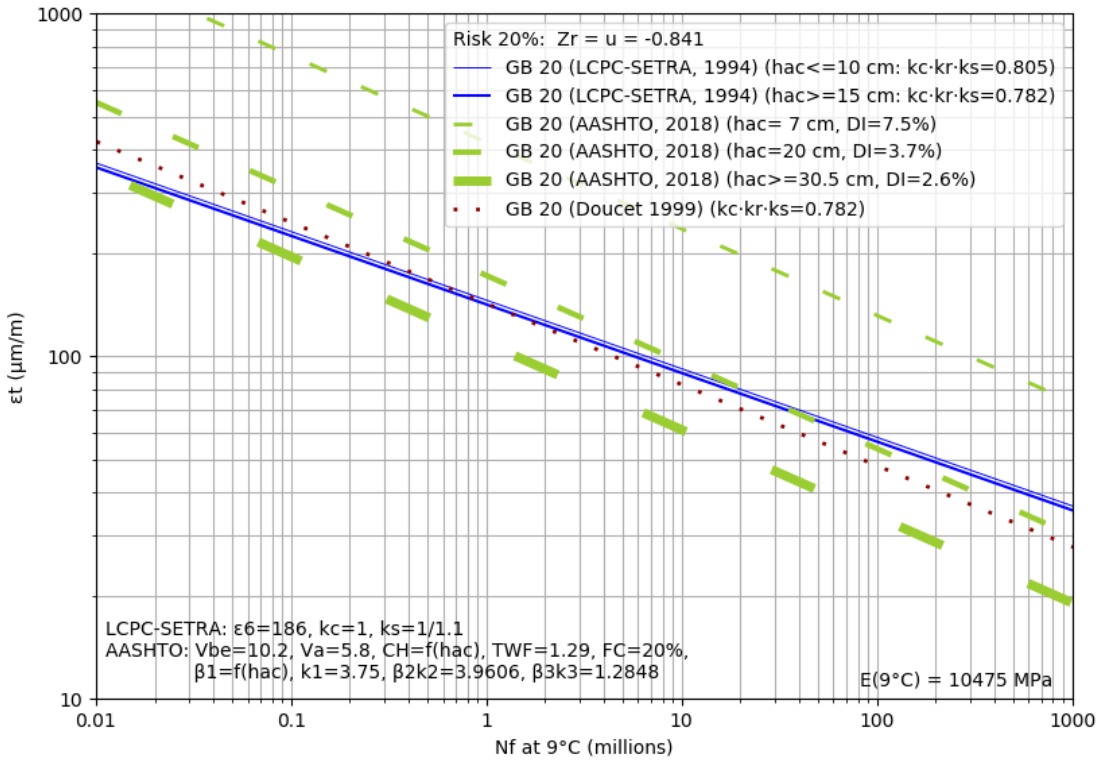


Figure 6. Correction factor for traffic wandering



a) GB 3 (Bordeaux)



b) GB 20 (SERUL)

Figure 7. Effective fatigue lines

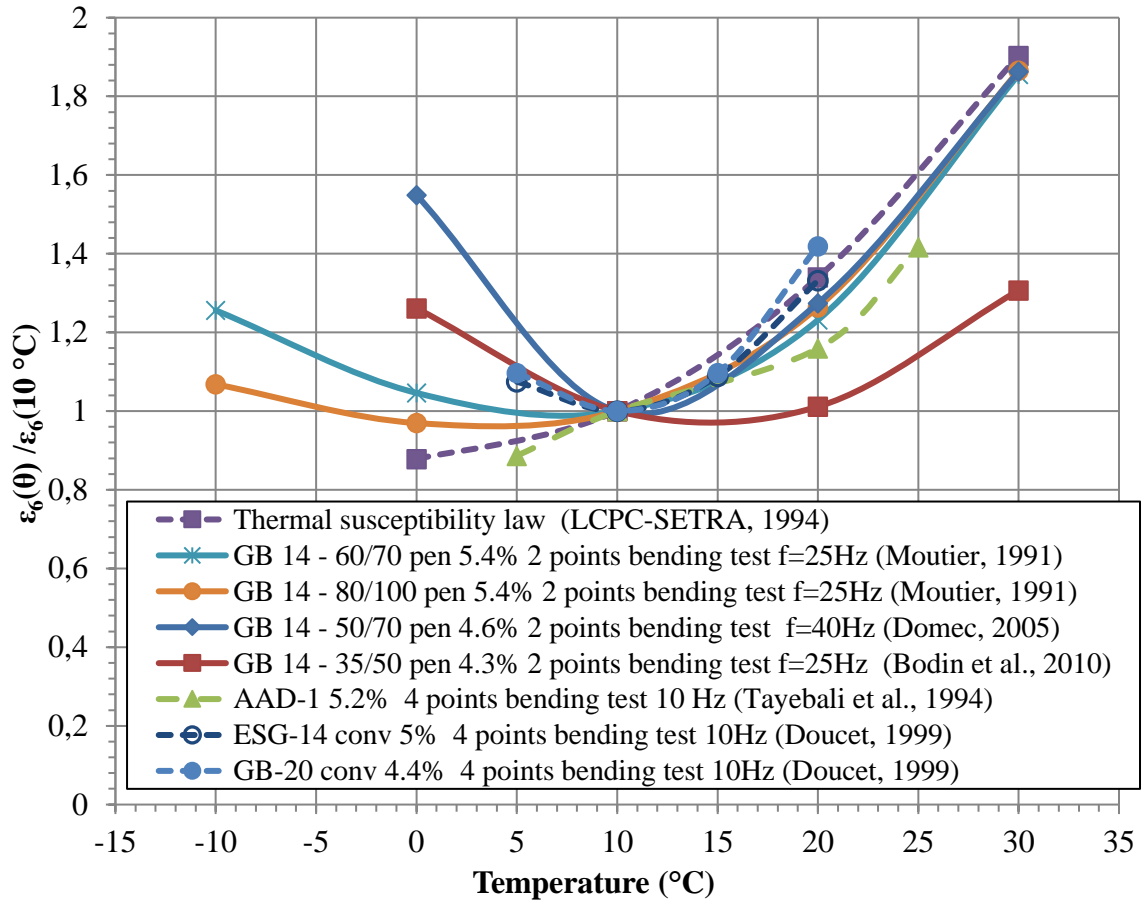


Figure 8. Changes in design parameter $\varepsilon_6(\theta)/\varepsilon_6(10\text{ }^\circ\text{C})$ as a function of temperature

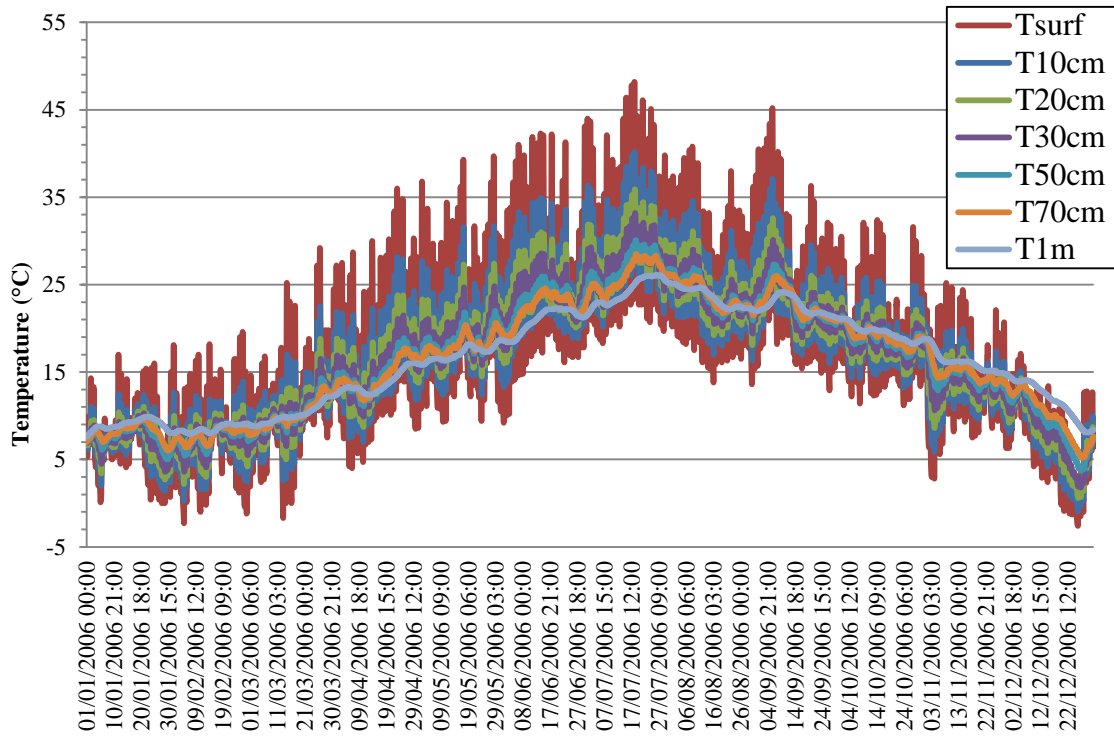


Figure 9. Changes in hourly temperature at various depths – A63 Bordeaux (2006)

Climate Station	
Elevation (m)	<input checked="" type="checkbox"/> 47
Climate station	<input checked="" type="checkbox"/> BORDEAUX,FR (047
Latitude (decimal deg)	<input checked="" type="checkbox"/> 44.83
Longitude (decimal de)	<input checked="" type="checkbox"/> -0.69
Depth of water table	<input checked="" type="checkbox"/> Annual(2)
Identifiers	
Approver	
Date approved	19/09/2017 3:08 PM
Author	
Date created	19/09/2017 3:08 PM
County	
Description of object	
Direction of travel	
Display name/identifi	
District	
From station (km)	
Item Locked?	False
Highway	
Revision Number	0
Province/State	

Climate Summary	
Mean annual air temperature (deg C)	13.8
Mean annual precipitation (mm)	839.6
Freezing index (deg C - days)	7.8
Average annual number of freeze/thaw cycles	24
Number of wet days	172.7
Monthly Temperatures	
Average temperature in January (deg C)	6.7
Average temperature in February (deg C)	6.7
Average temperature in March (deg C)	9.8
Average temperature in April (deg C)	13
Average temperature in May (deg C)	16
Average temperature in June (deg C)	20
Average temperature in July (deg C)	21.5
Average temperature in August (deg C)	21.1
Average temperature in September (deg C)	18.5
Average temperature in October (deg C)	14.8
Average temperature in November (deg C)	10.2
Average temperature in December (deg C)	6.7

Figure 10. Summary of climate data – A63 Bordeaux (2003-2016)

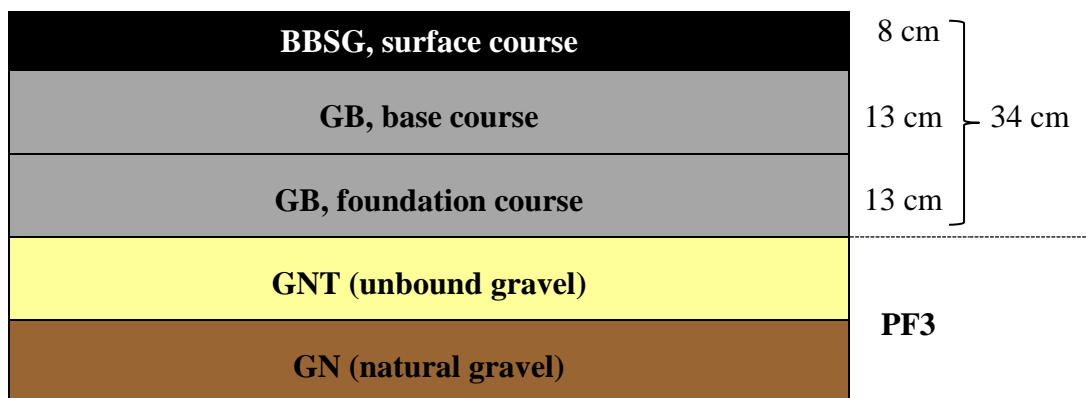


Figure 11. Pavement structure – A63 Bordeaux

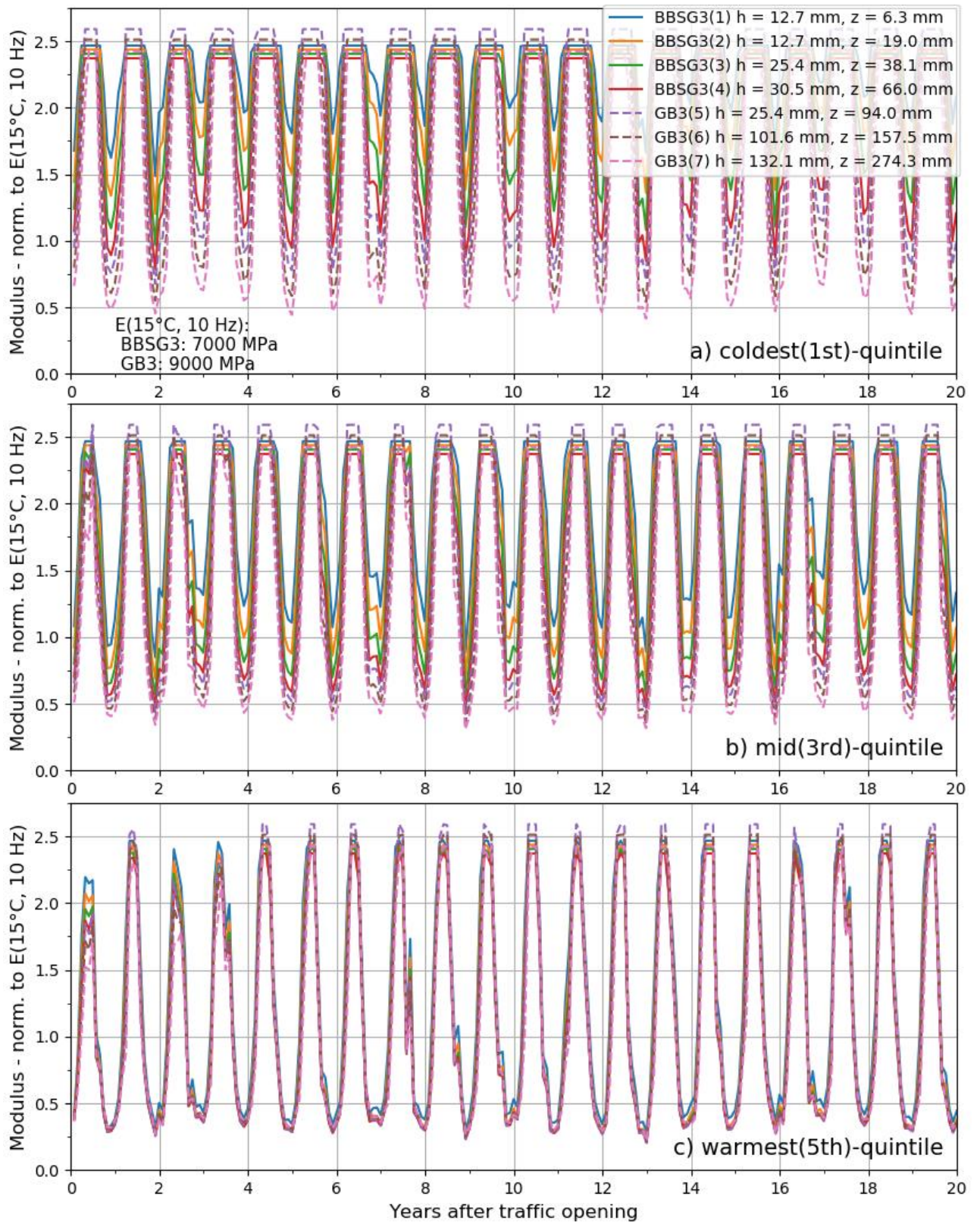
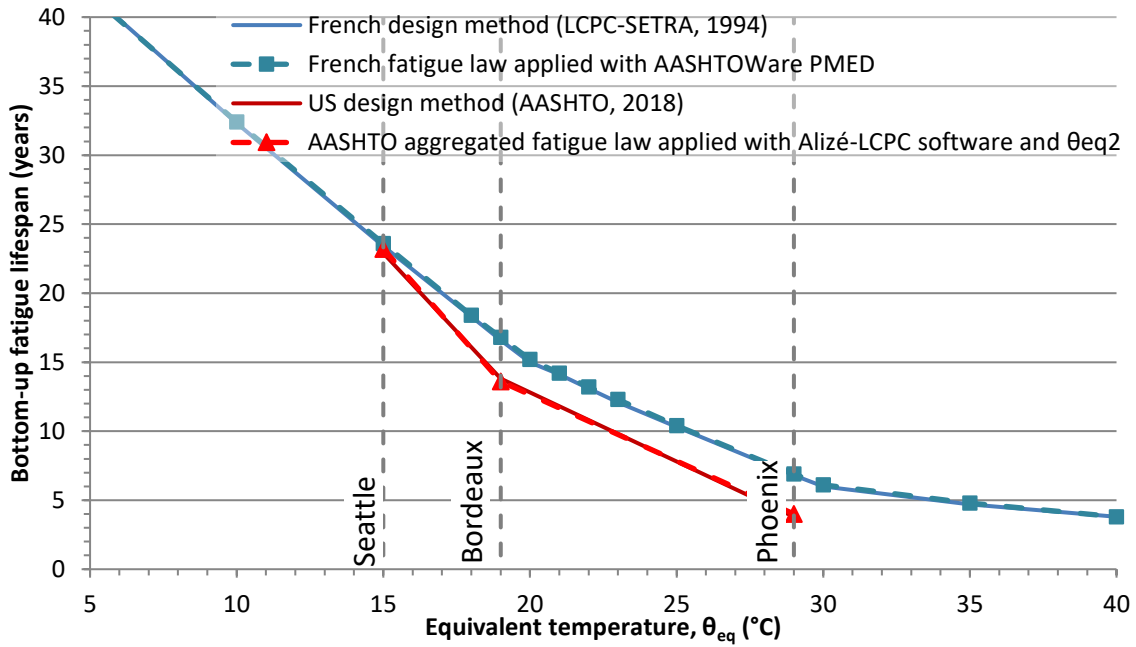
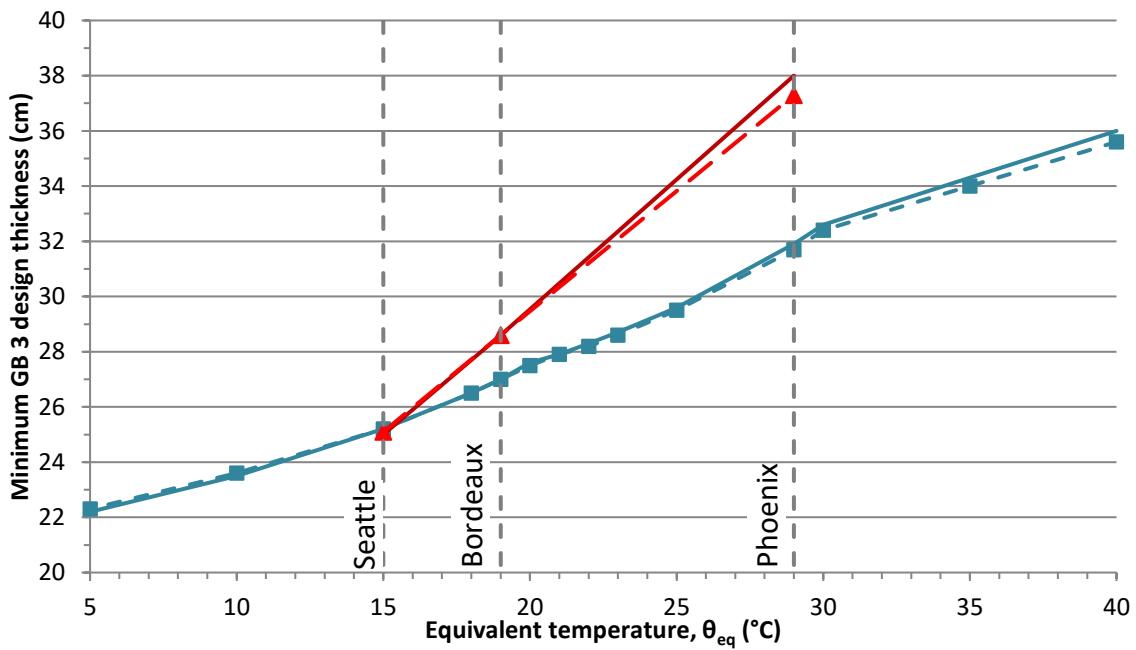


Figure 12. Simulation of moduli for bituminous layers – A63 Bordeaux (AASHTOWare PMED)



a) Lifespans



b) Thickness design

Figure 13. Summary of fatigue cracking results – A63

Climate Station	
Elevation (m)	<input checked="" type="checkbox"/> 672.8
Climate station	<input checked="" type="checkbox"/> SERUL.QC (04732)
Latitude (decimal deg)	<input checked="" type="checkbox"/> 47.32
Longitude (decimal deg)	<input checked="" type="checkbox"/> -71.15
Depth of water table	<input checked="" type="checkbox"/> Annual(1)
Identifiers	
Approver	
Date approved	26/09/2017 11:25 AM
Author	
Date created	26/09/2017 11:25 AM
County	
Description of object	
Direction of travel	
Display name/identifier	
District	
From station (km)	
Item Locked?	False
Highway	
Revision Number	0
Province/State	

Climate Summary	
Mean annual air temperature (deg C)	1.8
Mean annual precipitation (mm)	1392.5
Freezing index (deg C - days)	1557.9
Average annual number of freeze/thaw cycles	93.4
Number of wet days	238.4
Monthly Temperatures	
Average temperature in January (deg C)	-14.4
Average temperature in February (deg C)	-12.9
Average temperature in March (deg C)	-7.4
Average temperature in April (deg C)	-0.3
Average temperature in May (deg C)	7.8
Average temperature in June (deg C)	12.6
Average temperature in July (deg C)	15.4
Average temperature in August (deg C)	14.4
Average temperature in September (deg C)	10.1
Average temperature in October (deg C)	3.3
Average temperature in November (deg C)	-2.9
Average temperature in December (deg C)	-9.6

Figure 14. Summary of climate data – SERUL (2008-2016)

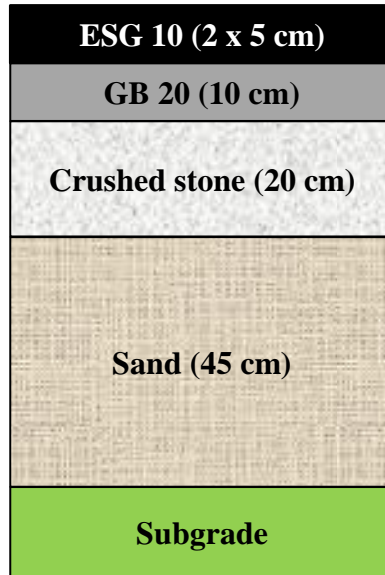
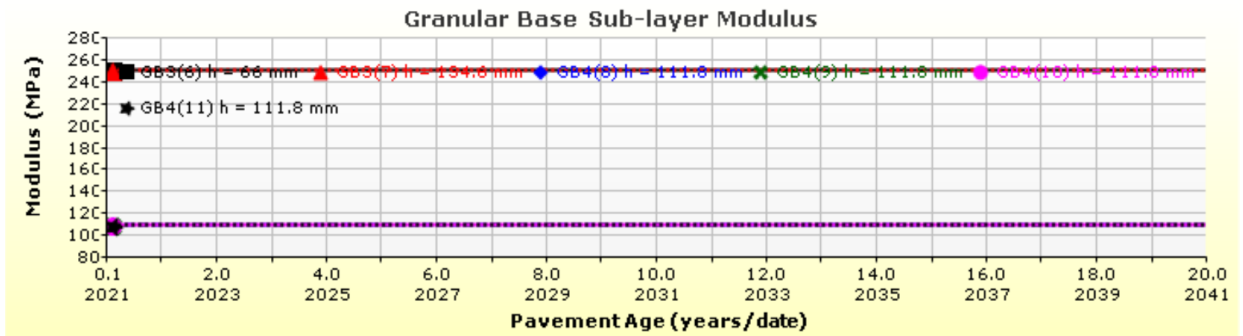
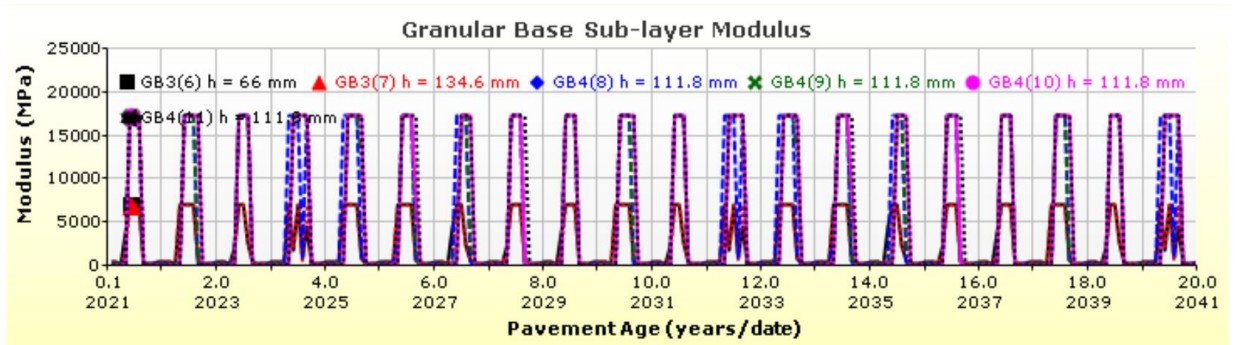


Figure 15. Pavement structure – SERUL (Badiane, 2016)



(a) Constant modulus (no freeze/thaw)



(b) Variable modulus (EICM model, freeze/thaw)

Figure 16. Changes in the unbound layer modulus – SERUL (AASHTOWare PMED)

Figure captions

Figure 1. Mechanistic-empirical design process (AASHTO, 2015)

Figure 2. Subdivision of a month into temperature quintiles (AASHTO, 2015)

Figure 3. Huet-Such model, (a) Representation (b) Expressions

Figure 4. Complex shear modulus master curve of binders in Black space

Figure 5. Aging simulation at a constant temperature of 15 °C (AASHTOWare PMED)

Figure 6. Correction factor for traffic wandering

Figure 7. Effective fatigue lines

Figure 8. Changes in design parameter $\varepsilon_6(\theta)/\varepsilon_6(10\text{ °C})$ as a function of temperature

Figure 9. Changes in hourly temperature at various depths – A63 Bordeaux (2006)

Figure 10. Summary of climate data – A63 Bordeaux (2003-2016)

Figure 11. Pavement structure – A63 Bordeaux

Figure 12. Simulation of moduli for bituminous layers – A63 Bordeaux (AASHTOWare PMED)

Figure 13. Summary of fatigue cracking results – A63

Figure 14. Summary of climate data – SERUL (2008-2016)

Figure 15. Pavement structure – SERUL (Badiane, 2016)

Figure 16. Changes in the unbound layer modulus – SERUL (AASHTOWare PMED)